COLLEGE OF EARTH AND MINERAL SCIENCES

Final Technical Report

Calculation of Source and Structure Parameters at Regional and Teleseismic Distances

Sponsored by
Advanced Research Projects Agency (DOD)
ARPA Order No. 4397
Monitored by AFOSR under Contract No. F49620-83-K-0019

Period of Performance
January 1, 1983 - March 31, 1985

Co-Investigators: Charles A. Langston
Roy J. Greenfield

May 31, 1985

The Pennsylvania State University

University Park, Pennsylvania

THE PENNSYLVANIA STATE UNIVERSITY

College of Earth and Mineral Sciences

UNDERGRADUATE PROGRAMS OF STUDY

Ceramic Science and Engineering, Earth Sciences, Fuel Science, Geography, Geosciences, Metallurgy, Meteorology, Mineral Economics, Mining Engineering, Petroleum and Natural Gas Engineering, and Polymer Science.

GRADUATE PROGRAMS AND FIELDS OF RESEARCH

Ceramic Science, Fuel Science, Geochemistry and Mineralogy, Geography, Geology, Geophysics, Metallurgy, Meteorology, Mineral Economics, Mineral Processing, Mining Engineering, Petroleum and Natural Gas Engineering, and Polymer Science.

UNIVERSITY-WIDE INTERDISCIPLINARY GRADUATE PROGRAMS INVOLVING E&MS FACULTY AND STUDENTS

Earth Sciences, Ecology, Environmental Pollution Control Engineering, Mineral Engineering Management, Operations Research, Regional Planning, and Solid State Science.

ASSOCIATE DEGREE PROGRAMS

Metallurgical Engineering Technology and Mining Technology.

INTERDISCIPLINARY RESEARCH GROUPS WITHIN THE COLLEGE

Coal Research Section, Mineral Conservation Section, Ore Deposits Research Section, and Mining and Mineral Resources Research Institute.

ANALYTICAL AND STRUCTURE STUDIES

Classical chemical analysis of metals and silicate and carbonate rocks; X-ray crystallography; electron microscopy and diffraction; electron microprobe analysis; atomic absorption analysis; spectrochemical analysis.

Final Technical Report

Calculation of Source and Structure Parameters at Regional and Teleseismic Distances

Sponsored by
Advanced Research Projects Agency (DOD)
ARPA Order No. 4397
Monitored by AFOSR under Contract No. F49620-83-K-0019

Period of Performance
January 1, 1983 - March 31, 1985

Co-Investigators: Charles A. Langston
Roy J. Greenfield

May 31, 1985

Unclassified

SECURITY CLASSIFICATION OF THIS PAGE (When Data Entered)

REPORT DOCUMENTATION PAGE	READ INSTRUCTIONS BEFORE COMPLETING FORM
1. REPORT NUMBER AFOSR-TR- 85-0753	2. GOVT ACCESSION NO. AD-A160 138
4. TITLE (and Subtitle) [redacted]: Calculation of Source and Structure Parameters at Regional and Teleseismic Distances	5. TYPE OF REPORT & PERIOD COVERED Final Technical Report Jan 1, 1983 - March 3, 1985
	6. PERFORMING ORG. REPORT NUMBER
7. AUTHOR(s) Charles A. Langston Roy J. Greenfield	8. CONTRACT OR GRANT NUMBER(s) F49620-83-K-0019
9. PERFORMING ORGANIZATION NAME AND ADDRESS The Pennsylvania State University University Park, PA 16802	10. PROGRAM ELEMENT, PROJECT, TASK AREA & WORK UNIT NUMBERS 61101F 2309/A1 [redacted]
11. CONTROLLING OFFICE NAME AND ADDRESS AFOSR / NP	12. REPORT DATE May 31, 1985
	13. NUMBER OF PAGES
14. MONITORING AGENCY NAME & ADDRESS (if different from Controlling Office) Building 410 Bolling AFB D.C. 20332-6448	15. SECURITY CLASS. (of this report) Unclassified
	15a. DECLASSIFICATION/DOWNGRADING SCHEDULE

16. DISTRIBUTION STATEMENT (of this Report)

Approved for public release; distribution unlimited.

17. DISTRIBUTION STATEMENT (of the abstract entered in Block 20, if different from Report)

18. SUPPLEMENTARY NOTES

19. KEY WORDS (Continue on reverse side if necessary and identify by block number)

SV waves, Ray theory, WKBJ approximation, body waves, crustal structure, upper mantle structure

20. ABSTRACT (Continue on reverse side if necessary and identify by block number)

Teleseismic SV waves have been generally ignored in wave propagation and source studies because of known complications in wave propagation for structure near the source and near the receiver. The validity of common optic ray and WKBJ seismogram methods for computing SV synthetic seismograms is examined by computing synthetic seismograms using these techniques and comparing them to SV synthetics produced from a wavenumber integration technique. Both ray methods give a poor approximation to the wave propagation for distances less than 60°. Diffracted Sp and the SPL wave interfer with near

DD FORM 1 JAN 73 1473 EDITION OF 1 NOV 65 IS OBSOLETE

Unclassified

SECURITY CLASSIFICATION OF THIS PAGE (When Data Entered)

source phases, such as S, pS, and sS for a shallow seismic source, producing anomalously high amplitudes and complex waveforms in agreement with observational experience. Because of the Moho Sp and diffracted Sp phases, the vertical component of motion shows greater distortion, relative to the ray theory result, than does the radial component of motion. Ray theory appears to be appropriate for the initial 20 seconds of the SV wavetrain from a shallow source for ranges greater than 60°. SV waves from deep sources are less affected by diffracted Sp and SPL than SV from shallow sources.

Diffracted Sp is found to be generated under the Australian shield by deep-seated Tonga, Honshu, and Bonin events. This seismic phase is set up at the Moho as a P head-wave by a critically-incident upgoing SV wave at an epicentral distance of around 50 degrees. The simple source time history inferred from P or SH particle motion and the absence of source structure effects on SV wave forms from a deep source suggest a diffracted Sp wave for the explanation of distorted SV waves recorded at the Mundaring station. The polarity of this phase arriving immediately after direct SV indicates a P-type of wave, excluding the possibility of other types of S waves like ScS. Using a WKBJ spectral method for SV wave propagation, synthetic seismograms for the direct SV and diffracted Sp are computed. With some modification of the P-velocity model by Mathur and the S-velocity model presented by Goncz & Cleary for the Australian shield, synthetics produce the distinctive interference between direct SV and diffracted Sp seen in the data. The arrival time difference between direct S and diffracted Sp is sensitive to the P-velocity of the upper mantle. Results of the analysis reveal a higher P-velocity structure of upper mantle in the southwestern shield than in the northwest. The analysis of teleseismic SV waveforms and the diffracted Sp phase is a new and useful technique for determining regional variations in upper mantle P velocity structure.

Body-wave forms from the eastern Hispaniola earthquake of September 14, 1981, were compared to synthetic seismograms to investigate the upper mantle P velocity structure of eastern North America. The event occurred at an intermediate depth, 190 km, ensuring that phases that arrived after direct P were sufficiently delayed that they did not interfere with the triplicated direct P phases. Triplicated phases are best observed in intermediate-period data. The lower discontinuity lies at 670 km, instead of at 650 km as in a published model for the region. The new velocity model is identical to the published model above 640 km.

Table of Contents

Summary

Work on this project has been concerned with a variety of source and related earth structure problems with emphasis on constructing synthetic seismograms for their solution. As presented in previous reports and publications as well as this report, we have worked in the following areas:

1. Moment Tensor inversions of earthquake data
2. The effect of structure perturbations on source parameters
3. The effect of spallation in the near-field of large underground explosions
4. Waveform inversion of sparse data sets from small events to determine source parameters
5. Analysis of crust and mantle structure under selected receivers
6. Constructing a method of computing teleseismic SV waves
7. Comparing this method to commonly used wave approximations
8. Using the Sp diffraction phase seen in teleseismic SV waveforms for a new method of determining upper mantle P velocity structure
9. Examining the upper mantle P velocity structure of eastern North America and the western Atlantic using triplication data.

The major goal of this work was to make progress in our understanding of wave propagation and seismic source parameters in order to be able to effectively model and understand observed seismic events. These results have direct application to the source discrimination problem. For example, a method has been implimented which makes possible the determination of accurate source parameters of small earthquakes from very limited teleseismic and regional data sets. Indeed, sometimes it is possible to determine source depth and focal mechanism from data recorded at a single receiver.

The structure problem always enters into the problem of source parameters. It is required that the effects of wave propagation must be known to understand the source effect in observed seismograms. In our work, we have concentrated in stuyding the structure effects of body wave propagation because body waves potentially allow higher resolution of source parameters than, say, surface waves. Source depth, in particular, is an important parameter to discriminate between explosions and earthquakes. Teleseismic body waves are very good data to examine and to determine source depth because of the distinctive interference of pP and P. Thus, it is always important to determine the effects of structure in the crust and mantle to be included in the necessary wave responses for source excitation.

In this report we present three studies related to both source and structure problems. In the first (page 1), we examine the validity of common optic ray and asymptotic ray approximations in the computation of SV waves. SV waves have been generally ignored in seismological studies because of

complicated structure effects near the source and receiver which serve to obscure the direct SV wave at most teleseismic distances. The SV wave is increasingly being recognized, however, as being important in the source problem. Not only is it a data source to be utilized in conjunction with P, SH, and surface waves in determining earthquake source parameters, the use of SV wave may also represent a way of determining the non-isotropic components of explosion sources. This is a particularly relevant issue in the yield determination of underground explosions. The results of the comparison of three methods of computing teleseismic SV waves show that crustal and upper mantle structure effects are important and that simple ray methods do not adequately simulate the actual response. The ray method results were compared to the WKBJ spectral method for computing SV waves developed early in this project.

In the second study, we examine the utility of using structural phases observed in the teleseismic SV wave to actually determine mantle structure. The experiment (page 24) consisted of collecting teleseismic SV waves from deep events recorded at the Australian WWSSN receiver MUN (Mundaring) and modeling the waveforms using the WKBJ spectral technique. The observed waves showed a distinctive P wave arriving after the direct S wave that could not be attributed to the source or near-receiver structure. This P wave is the Sp diffraction which is set up at distances of 50 degrees or so from the source and propagates in the uppermost mantle, similar to the regional phase Pn, to the receiver at farther distances. Like Pn, the relative arrival time of the Sp diffraction allows the upper mantle P wave velocity to be estimated. It was found that the upper mantle west of MUN contained high P velocities of 8.3 to 8.4 km/sec in comparison to the upper mantle north of the station which had velocities of only 8.1 to 8.2 km/sec. The high velocities are consistent with previous regional refraction experiments and the differences seen with travel path were consistent with variations in the regional heat flow. The use of the Sp diffraction phase contained within the teleseismic P waveform is an interesting new addition to the tools available for determining mantle structure. In a sense, the teleseismic data enables one to construct regional refraction profiles in areas otherwise inaccessible. This has obvious utility in determining structure in parts of Asia.

The third study presented here (page 57) is of a standard analysis of upper mantle triplication data recorded in Eastern North America from an intermediate depth earthquake in the Carribbean. The principal result was the 650 km depth discontinuity in the upper mantle determined by Burdick in the area had to be lowered to 670 km to explain the triplication data. The rationale for using this particular event was the fact that the effective source function was much simpler than that of a shallow earthquake because the direct wave was well separated from the surface reflections. The hope was to examine the triplications without the extra near-source complexity to obscure the waveform. The effect of the triplications in the long-period data was evident yet subtle. It was seen, however, that broad-band data from the RSTN was ideal in resolving the relative timing and amplitude of the triplications.

The Validity of Ray Theory Approximations for the Computation of Teleseismic SV Waves

by Charles A. Langston

and

Chang-Eob Baag

Department of Geosciences

The Pennsylvania State University

University Park, PA 16802

March 6, 1985

Abstract

Teleseismic SV waves have been generally ignored in wave propagation and source studies because of known complications in wave propagation for structure near the source and near the receiver. The validity of common optic ray and WKBJ seismogram methods for computing SV synthetic seismograms is examined by computing synthetic seismograms using these techniques and comparing them to SV synthetics produced from a wavenumber integration technique. Both ray methods give a poor approximation to the wave propagation for distances less than 50°. Diffracted Sp and the SPL wave interfere with near source phases, such as S, pS, and sS for a shallow seismic source, producing anomalously high amplitudes and complex waveforms in agreement with observational experience. Because of the Moho Sp and diffracted Sp phases, the vertical component of motion shows greater distortion, relative to the ray theory result, than does the radial component of motion. Ray theory appears to be appropriate for the initial 20 seconds of the SV wavetrain from a shallow source for ranges greater than 60°. SV waves from deep sources are less affected by diffracted Sp and SPL than SV from shallow sources.

Introduction

The modeling of P and SH long-period waveform data in the inversion of source parameters has become a standard technique in source inversion studies. Because the propagation of these body waves is relatively simple for teleseismic distances, the interference of near-source phases such as P and pP can be easily utilized to estimate source depth, time function, and orientation parameters. Waveform shape is mostly controlled by near-source interactions with the effect of the mantle and receiver structure represented by a geometric spreading factor and attenuation operator. Ray theory or the saddle point approximation of a Thomson-Haskell formulation is often used to compute the neccessary Green's functions needed for source inversion algorithms. Because these methods are computationally undemanding, they are well suited for iterative source inversion. Many recent investigators have used teleseismic body wave inversion algorithms based on a moment tensor parameterization with success(e.g., Fitch et al, 1980; Ward, 1980; Langston et al, 1982; Nabelek, 1984).

In contrast with the relative simplicity of teleseismic P and SH waveforms, the teleseismic SV waveform is difficult to work with because of known complications in SV wave propagation. Figure 1 displays a travel time curve for the direct SV wave from a 15km depth source between the ranges of about 15 degrees to 100 degrees. Also shown are the expected

arrival times of ScS and SKS. On the basis of this curve it would appear that the SV waveform should be relatively uncontaminated by other mantle and core arrivals between the ranges of 30 and 75 degrees. However, it is seen observationally that the "SV" wave displays elliptical and complex particle motion not in accord with the expected rectilinear motion from a simple body wave.

This behavior is due to the excitation of the shear-coupled PL wave (Oliver, 1961) and the Sp diffraction (Frazer, 1977). These waves are set up in the crust and upper mantle near the receiver for a deep source. Wave propagation from a crustal source is much more complicated since both kinds of waves are excited in structure near the source as well as near the receiver (Baag and Langston, 1985a; 1985b).

The SV waveform has been generally avoided in source studies because of this complex behavior. An exception to this is the method of Dziewonski et al (1981) who utilize a modal summation to construct the Green's functions for the entire seismogram at long periods. The purpose of this paper is to examine the accuracy of the ray approximation in the computation of SV waves at teleseismic distances. This is naturally important for those inversion methods which utilize ray theory since the SV waveform represents an additional set of data to constrain source parameters. Further, ray methods are generally easier to implement than normal modes for

computations at high frequencies. This is an important factor when using short-period or broad-band seismic data.

Synthetic seismograms will be constructed using three different methods. The wavenumber integration method of Baag and Langston(1985b) will provide the canonical set of synthetic seismograms containing the complexities of SPL and diffracted Sp wave propagation. These will be directly compared to synthetic seismograms computed using optic ray theory and Chapman's (1978) WKBJ seismogram method. Considering a crustal source, it will be seen that the ray methods may be appropriate only for modelling the SV waveform at distances greater than 60 degrees. At closer ranges ray theory may be adequate only for the initial half cycle of the SV wave.

Method

Baag and Langston(1985a,b) describe a wavenumber integration technique for computing teleseismic SV waves and related source and receiver effects which produce the SPL phase. Basically, the spectrum of vertical or radial displacement, $u(\omega)$, is given by an integral of the form

$$u(\omega) = \int_{p1}^{p2} F(p,\omega) J_n(\omega p r) dp \qquad (1)$$

where, J_n is a Bessel function of order n, $F(p,\omega)$ is the vertical wave function containing source and structure model parameters, p is ray parameter, r is radial distance in

a cylindrical coordinate system, and ω is circular frequency. Horizontal wavenumber is given by ωp. The integral is evaluated over an appropriate range of ray parameter which includes the phases of interest for a particular receiver distance. The structure model is parameterized such that the crust and a portion of the upper mantle at the source and receiver is represented by discrete homogeneous layers. Mantle structure beneath the upper layers is given by a continuous vertically inhomogeneous velocity function. Attenuation is explicitely included in the model using complex-valued velocity. The vertical wave function, $F(p,\omega)$ is computed using Thomson-Haskell layer matices for the layered part of the model and the spectral WKBJ approximation for the vertically inhomogeneous part. An earth-flattening transformation is used to compute responses for a spherical earth model. Details of the method can be found in Baag and Langston(1985b). This method will be used to create accurate synthetic seismograms containing the effects of the "leaky mode" SPL phase and the diffracted Sp wave to be compared with ray theory results.

The geometrical ray theory formulation of Langston and Helmberger(1975) for the teleseismic SV response due to a crustal dislocation source is given by

$$u(t) = R_{SR}[\dot{\Omega}(t) + R_{SS}\dot{\Omega}(t - t_1) + R_{PS}(n_\beta/n_\alpha)\dot{\phi}(t - t_2)] * S(t) * Q(t) * I(t) \quad (2)$$

where, R_{ss} is the receiver function, R_{ss} is the free surface S-to-S reflection coefficient, and R_{ps} is the free surface P-to-S reflection coefficient. $\dot{\Omega}$ and $\dot{\phi}$ are the time derivatives of the SV and P wave potentials, respectively. The quantities t_1 and t_2 are the lag times for sS and pS relative to direct S, respectively. S(t), Q(t), and I(t) are far-field source time function, attenuation operator and instrument response operator, respectively. The ratio of vertical S slowness to P slowness, (η_β/η_α), is the geometrical spreading correction for phase conversion.

It is assumed in the geometrical ray calculations that structure near the source and receiver is simply a homogeneous half-space. This is an ideal case that is often used to compute the response of teleseismic P and SH waves, particularly where the source crust is simple. This assumption is often good for these waves since the effect of crustal reverberations is usually small at long periods.

Obviously, geometrical ray theory can be used to compute the effect of near-source reverberations as well as receiver conversions and reverberations. Rather than do this, we will employ Chapman's (1978) WKBJ seismogram method to include these phases. The WKBJ seismogram computation involves summing a series of generalized rays appropriate for the structure and section of the seismogram under consideration. In theory, the WKBJ seismogram technique is more robust than the geometrical ray method since it can give the response due

to diffracted waves such as head waves and diffractions from the cusps of triplications. Thus, it might be expected that the WKBJ seismogram would give a more accurate synthetic than one computed from geometrical ray theory.

After Chapman(1978), the WKBJ seismogram is given by

$$u(t) = -\mathrm{Im}\left\{ S(t) *_t \sum_{\theta} \frac{p^{1/2} R(p) K(p)}{|d\theta/dp|} \right\} * Q(t) * I(t) \qquad (3)$$

where,

$$S(t) = s(t) - i\,\mathcal{H}[s(t)]$$

and

$$s(t) = \frac{M_o}{4\pi} S_f(t) * \left[\frac{1}{\pi\sqrt{2r}} \quad \frac{H(t)}{\sqrt{t}} \right]$$

S(t) is the analytic time function and $\mathcal{H}[\,]$ is the Hilbert transform. Here, $S_f(t)$ is the far-field source time function, R(p) is the product of reflection/transmission coefficients for the generalized ray, and K(p) is a source factor. $\theta(p)$ is the travel time equation for the particular ray under study.

The model parameterizaton of velocity for the variation of the WKBJ seismogram method used here is identical to that of the wavenumber integration method. Plane layers as well as continuous velocity functions represent the earth model. An earth flattening approximation is also used to compute the response of a spherical earth model. In the computations

that follow, 36 generalized rays will be included in the WKBJ responses. These include the free surface reflections and one reverberation of the SV wave in the source and receiver crust. The major P-to-SV and SV-to-P conversions in both structures are also included. These rays are chosen to produce an accurate response for the first 30 seconds of the SV body wave. Other higher order reverberations and conversions were tested to see if they contributed the response. At most ranges, roughly 50% of the rays included in the final responses have amplitudes 10% or less than the largest amplitude.

Results

Synthetic seismograms were calculated for the three fundemental sources needed to construct an arbitrarily oriented dislocation or deviatoric moment tensor source (Langston, 1981). These are the vertical strike-slip, vertical dip-slip and 45 degree dip-slip terms of the dislocation and moment tensor formulations. Source depth was taken to be 15km in an earth model, SNA, developed from SH wave travel-time and waveform data by Grand and Helmberger(1984). The WWSSN long-period instrument response(T_a=100 sec, T_s=15 sec) and a trapezoidal far-field time function were convolved with all earth responses. In addition, the ray method results included a convolution with a Futterman(1962) attenuation operator. To be consistent with the attenuation structure assumed in the wavenumber

integration, a T/Q ratio of 4.5 was assumed. The trapezoidal time function had rise, constant level, and fall-off time durations of 1., 3., and 1. seconds, respectively.

Figure 2 shows detail of the complexity of the SV waveform for the 45 degree dip-slip source at 60 degrees distance. These waveforms were constructed using the wavenumber integration(WI) method and contain all propagation effects. A time increment of 2 seconds was used in all WI synthetics which accounts for the sharpness of some peaks and troughs in the figures.

Both components of ground motion show complicated wave motion. The first arrival is the S-to-P conversion and P-to-S conversion at the Moho of the receiver and source crust, respectively, although the receiver conversion predominates. The arrival labeled "S" is actually composed of near source phases S, sS, and pS interfering with each other. Immediately after S is the Sp diffraction which produces the relatively high frequency sinusoidal motion on the vertical component. This phase was studied by Frazer(1977) and Baag and Langston(1985a). It is set up in the uppermost mantle by an incident SV wave inside the range of 45 to 50 degrees. The SV wave converts to a P wave which travels horizontally below the Moho not unlike the P_n head wave. Depending on the velocity gradient in the upper mantle, this wave may take on the attributes of a "whispering gallery" phase in that multiple reflections and turning

points may occur. The Sp diffraction grades into the SPL phase which is the large long-period sinusoid in the remainder of the waveforms. Particle motion of SPL is prograde elliptical.

From a ray theory point of view, these phases are set up when the incident SV wave has a ray parameter greater than 1/8 sec/km, i.e., for receiver distances less than 45 degrees. Converted P waves get trapped in the crust and upper-most mantle and then propagate with a phase velocity roughly that of upper mantle P velocity. If crustal structure is relatively homogeneous and continuous over distances of approximately 30 degrees, the SPL and the Sp diffraction may be prominent out to distances of 70 degrees or more (Baag and Langston, 1985a).

Figure 3 shows the comparison of synthetic seismograms computed using wavenumber integration(WI), WKBJ seismogram method(WKBJ), and ray theory or the first motion approximation method(FMA). Vertical and radial displacements for the three fundemental source terms are shown since each source excites the SV wave in different ways. The FMA seismograms are all relatively simple since they only contain the direct wave and surface reflections near the source. It is assumed that the receiver structure is a homogeneous half-space. The WKBJ synthetics include the effect of receiver structure. At ranges of 70 degrees or more, the effect of receiver structure is primarily shown by the Sp

precursor phase. In all WKBJ cases it shows up as a small phase of the same polarity as S on the vertical component and of opposite polarity on the radial just before the S arrival. Compare Figure 2 with Figure 3 for example. Other than this Sp phase, the WKBJ synthetics closely match the amplitude and shape of FMA synthetics at the three farther ranges. This is particularly true of the radial components since Sp is small compared to S.

At ranges of 80 and 90 degress, SPL and the Sp diffraction phases occur late in time, relative to direct S, so the WI synthetics generally match the WKBJ synthetics. At closer ranges SPL and diffracted Sp significantly interfere with the SV body wave to produce varying levels of distortion of the waveform among the three fundemental sources. Note, for example, the 30 to 50 degree cases where these phases produce very complex vertical and radial waveforms. The Sp diffraction is most pronounced for the 45 degree dip-slip source for the vertical component at close ranges.

The WKBJ seismograms are principally affected by the phase shifts due to complex transmission and conversion coefficients at close ranges. However, the synthetics for 30 degrees range show a shortcoming of the WKBJ method. The diffraction from the cusp of the triplication from the 670 km discontinuity dominates the waveform as a second arrival. This is the cause, for example, of apparently large amplitudes seen in 45 degree dip-slip case(Figure 3c).

Inclusion of the WKBJ approximation in the wavenumber integration method does not give rise to this effect as shown in Baag and Langston(1985b).

Discussion and Conclusions

The comparison of synthetics in Figure 3 shows that there are ranges and time intervals in which ray methods are sufficient for the task of computing accurate Green's functions describing the wave propagation. The first 30 seconds of the waveform at ranges of 70 to 90 degrees appear to be usefully modelled using geometrical or WKBJ ray theory. At some closer ranges, the WKBJ technique appears to be adequate provided the appropriate rays for source and receiver structure are included and only the first half cycle of the SV waveform is considered. Even at 60 degrees distance, however, the radial displacement for the vertical strike-slip term is contaminated with the SPL phase early in the waveform (Figure 3a). At 30 and 40 degrees distance it appears that the wavenumber integration method must be used to produce the Green's function since both amplitude and waveshape appear to be severely affected by non-geometrical wave effects.

At ranges less than 50 degrees the WKBJ seismogram method as used here clearly only gives the initial portion of the waveform since the number of rays is practically limited by computational considerations. Converted S-to-P waves will increasingly become important for these distances since they

become trapped in the source and receiver crusts by the critical angle at the Moho. At ranges greater than or equal to 50 degrees these rays do not become trapped in the crust from conversion from the direct SV wave. However, the SPL wave can be thought of as result of these converted waves interfering with each other at closer distances and propagating to greater distances in the crustal waveguide. These effects are similar to the excitation of higher mode surface waves which is impossible or exceptionally difficult to compute with ray or generalized ray theory.

The severity of these effects will change with frequency or the pass-band of the recording instrument. The SPL phase response can be expected to decrease significantly at high frequencies so that the contamination for short-period or intermendiate-period records will be much less than seen here. However, the Sp diffraction may still be a significant arrival even at high frequencies. This depends on the crustal and upper mantle velocity structure over which it propagates. It may be expected that positive velocity gradients in the structure below the Moho will produce turning points for P waves composing the diffracted Sp phase which will cause these P waves to be strong at high frequency (Frazer, 1977; Baag and Langston, 1985b). In any event, these effects must be considered for any SV data set before relying on a ray theory approximation in the computation of

the Green's functions.

In this study we have explicitely considered a crustal source in which reverberations and wave effects are equally strong in the source and receiver structure. Baag and Langston(1985a) show that the SPL and diffracted Sp waves are less severe for mantle depth sources. Although the relative timing of these phases is the same for deep and shallow sources, excitation is confined to the structure in the vicinity of the receiver. Synthetic calculations show that SPL and diffracted Sp are smaller than their shallow source counterparts by factors of 2 to 10, with relative amplitude decreasing with range. Thus, the SV body wave dominates the waveform at most ranges for a deep source. The use of ray theory for the study of SV waves from deep sources may be more justified for ranges starting at 50 degrees but data will still be significantly contaminated by non-ray effects.

Acknowledgements

This research was supported by the Advanced Research Projects Agency of the Department of Defense and was monitored by the Air Force Office of Scientific Research under Contract #F49620-83-K-0019.

References

Baag, Chang-Eob and C. A. Langston(1985a). Shear-coupled PL, Geophysical J. R. astr. Soc., 80, 363-386.

Baag, Chang-Eob and C. A. Langston(1985b). A WKBJ spectral method for computation of SV synthetic seismograms in a cylindrically symmetric medium, Geophysical J. R. astr. Soc., 80, 387-418.

Chapman, C.H.(1978). A new method for computing synthetic seismograms, Geophysical J. R. astr. Soc., 54, 481-518.

Dziewonski, A.M., A.L. Hales and E.R. Lapwood(1975). Parametrically simple earth model consistent with geophysical data, Phys. Earth Planet. Int., 10, 12-48.

Dziewonski, A.M., T.A. Chou and J.H. Woodhouse(1981). Determination of earthquake source parameters from waveform data for studies of global and regional seismicity, J. Geophys. Res., 86, 2825-2852.

Fitch, T.J., D.W. McCowan, M.W. Shields(1980). Estimation of the seismic moment tensor from teleseismic body wave data with applications to intraplate and mantle earthquakes., J. Geophys. Res., 85, 3817-3828.

Frazer, L.N.(1977). Synthesis of shear coupled PL, Ph.D. Thesis, Princeton University.

Futterman, W.I.(1962). Dispersive body waves, J. Geophys. Res., 67, 5279-5291.

Grand, S.P. and D.V. Helmberger(1984). Upper mantle shear structure of North America, Geophyscal J. R. astr. Soc., 76, 399-438.

Langston, C.A.(1981). Source inversion of seismic waveforms: The Koyna, India, earthquakes of 13 September 1967, Bull. Seismol. Soc. Am., 71, 1-24.

Langston, C.A. and D.V. Helmberger(1975). A procedure for modelling shallow dislocation sources, Geophysical J. R. astr. Soc., 42, 117-130.

Langston, C.A., J.S. Barker, and G.B. Pavlin(1982). Point source inversion techniques, Phys. Earth Planet. Int., 30, 228-241.

Nabelek, J.L.(1984). Determination of earthquake source parameters from inversion of body waves, Ph.D. Thesis, Massachusetts Institute of Technology, Cambridge, Mass.

Oliver, J.(1961). On the long period character of shear waves, Bull. Seismol. Soc. Am., 51, 1-12.

Ward, S.N.(1980). A technique for the recovery of the seismic moment tensor applied to the Oaxaca, Mexico earthquake of November, 1978, Bull. Seismol. Soc. Am., 70, 717-734.

Figure Captions

Figure 1: Reduced travel-time distance curve for the direct SV wave from a 15 km depth source. Also shown are the curves for ScS and SKS. The crust and upper mantle model is Grand and Helmberger's(1984) SNA structure. A Jeffreys-Bullen lower mantle overlies core structure taken from the PEM model of Dziewonski et al(1975). This structure was used in the wavenumber integration and WKBJ seismogram calculations.

Figure 2: Radial and vertical displacement for the SV wavetrain from the 45 degree dip-slip source at 60 degrees distance. Major phases are shown on the waveforms and are discussed in the text.

Figure 3: Comparison of SV waveforms computed using the wavenumber integration technique(WI), WKBJ seismogram method(WKBJ), and first motion approximation method(FMA). Distance is shown in degrees and amplitudes are in microns. Waveforms from the vertical strike-slip, vertical dip-slip, and 45 degree dip-slip sources are given in Figures 3a, 3b,and 3c, respectively. A scalar source moment of $1x10^{25}$ dyne-cm was assumed in the calculations.

ScS
SKS
S
0
10
20
30
40
50
60
70
80
90
DISTANCE (DEGREES)
0
50
100
150
200
250
300
350
TRAVEL TIME - Δ x 13.9 (SEC)

FIG. 1

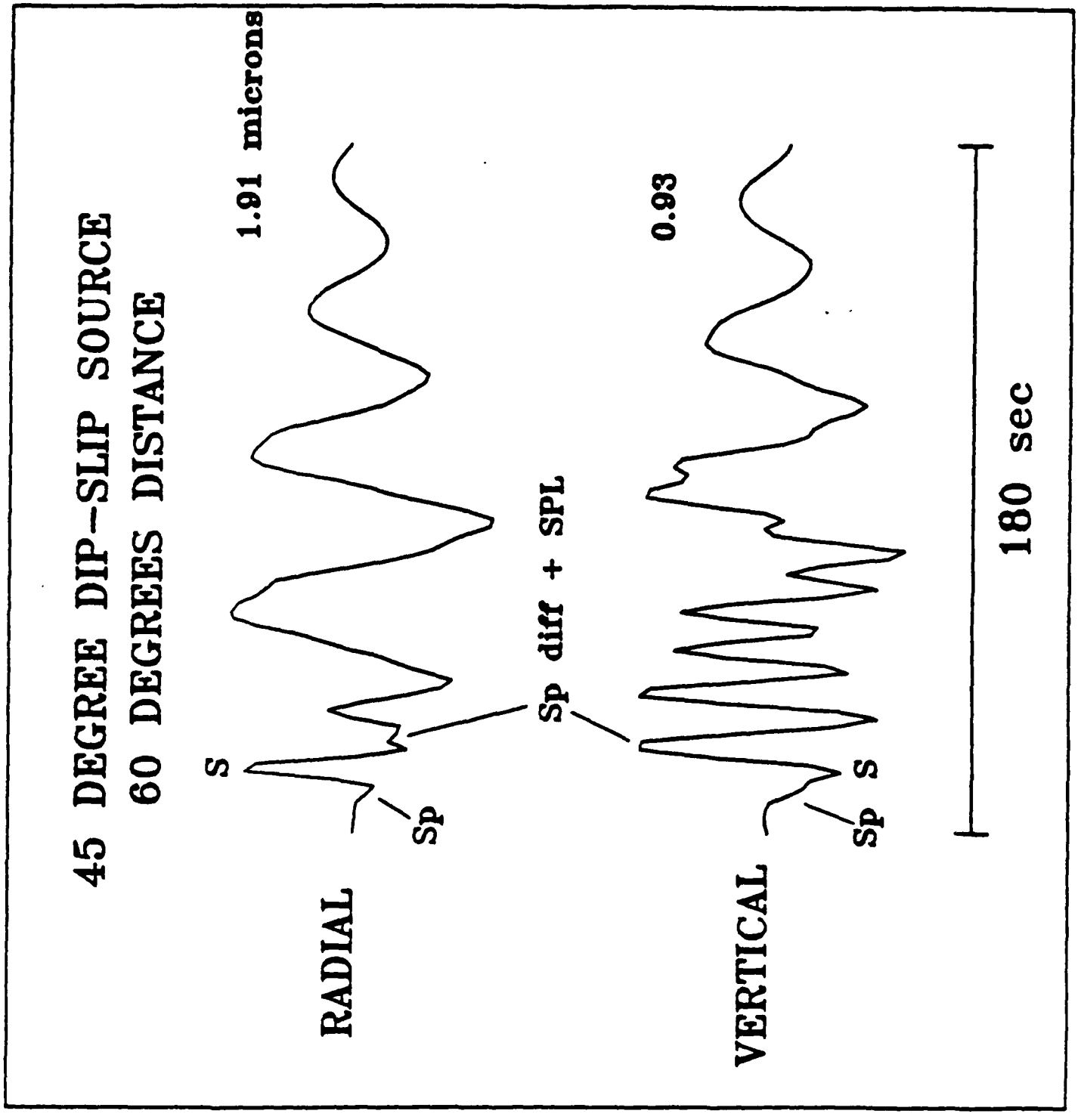
45 DEGREE DIP-SLIP SOURCE
60 DEGREES DISTANCE
1.91 microns
RADIAL
S
Sp
Sp diff + SPL
0.93
VERTICAL
Sp S
180 sec

FIG. 2

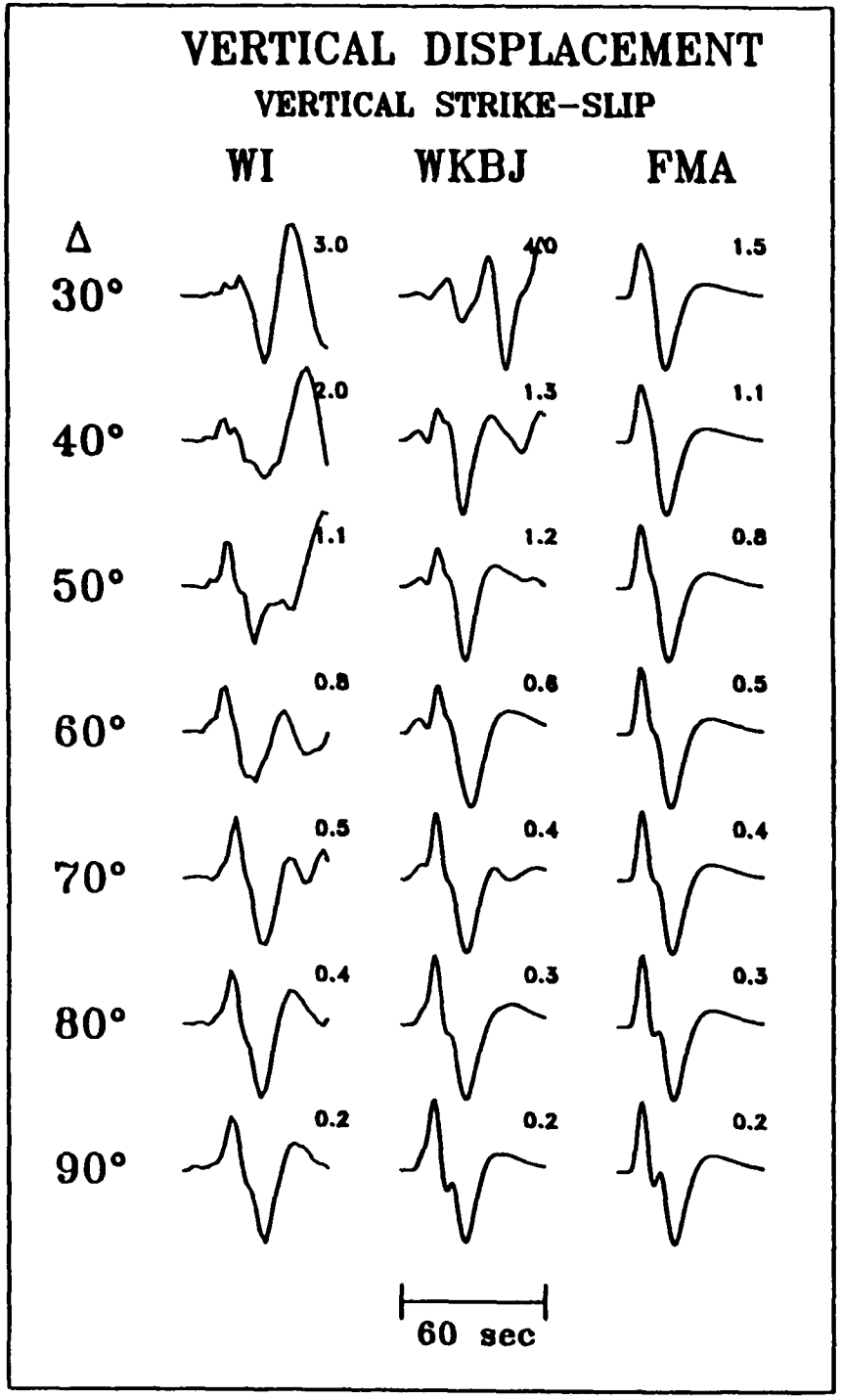
VERTICAL DISPLACEMENT
VERTICAL STRIKE-SLIP
WI
WKBJ
FMA
Δ
30°
40°
50°
60°
70°
80°
90°
3.0
4.0
1.5
2.0
1.3
1.1
1.1
1.2
0.8
0.8
0.6
0.5
0.5
0.4
0.4
0.4
0.3
0.3
0.2
0.2
0.2
60 sec

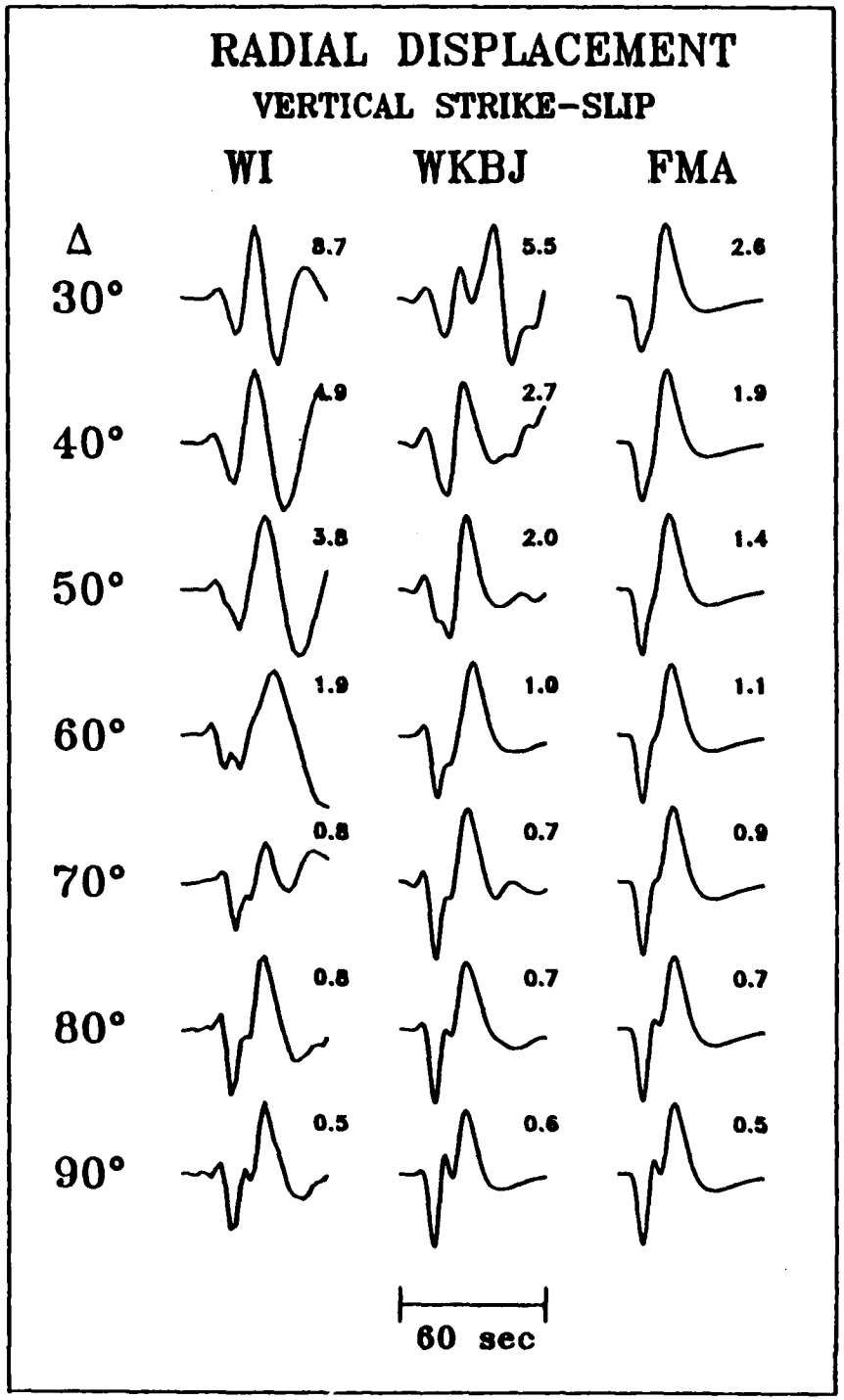
RADIAL DISPLACEMENT
VERTICAL STRIKE-SLIP
WI
WKBJ
FMA
Δ
30°
40°
50°
60°
70°
80°
90°
8.7
5.5
2.6
4.9
2.7
1.9
3.8
2.0
1.4
1.9
1.0
1.1
0.8
0.7
0.9
0.8
0.7
0.7
0.5
0.6
0.5
60 sec

FIG. 2a

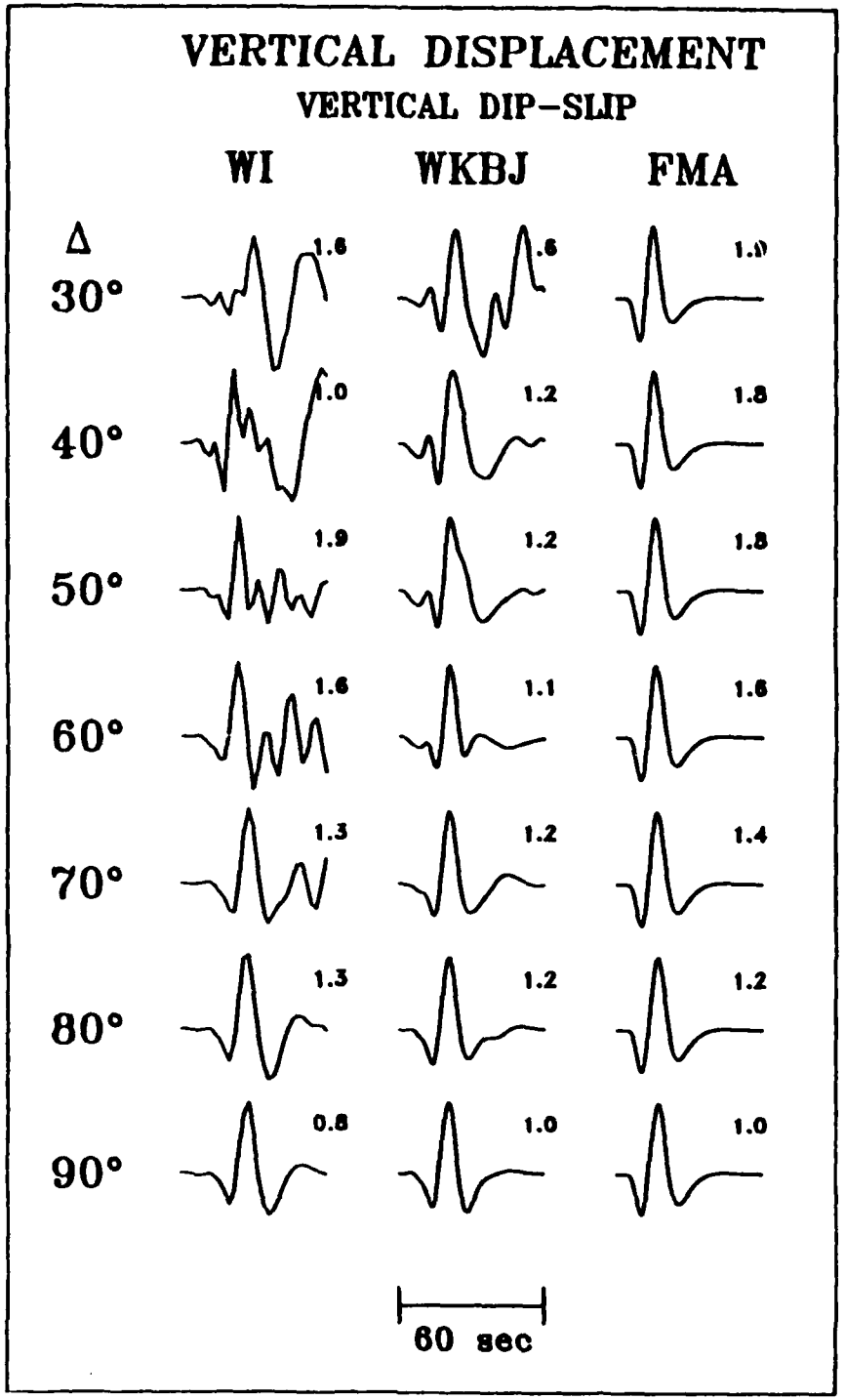
VERTICAL DISPLACEMENT
VERTICAL DIP-SLIP
WI
WKBJ
FMA
Δ
30°
40°
50°
60°
70°
80°
90°
1.6
1.0
1.9
1.6
1.3
1.3
0.8
1.2
1.2
1.1
1.2
1.2
1.0
1.8
1.8
1.8
1.4
1.2
1.0
60 sec

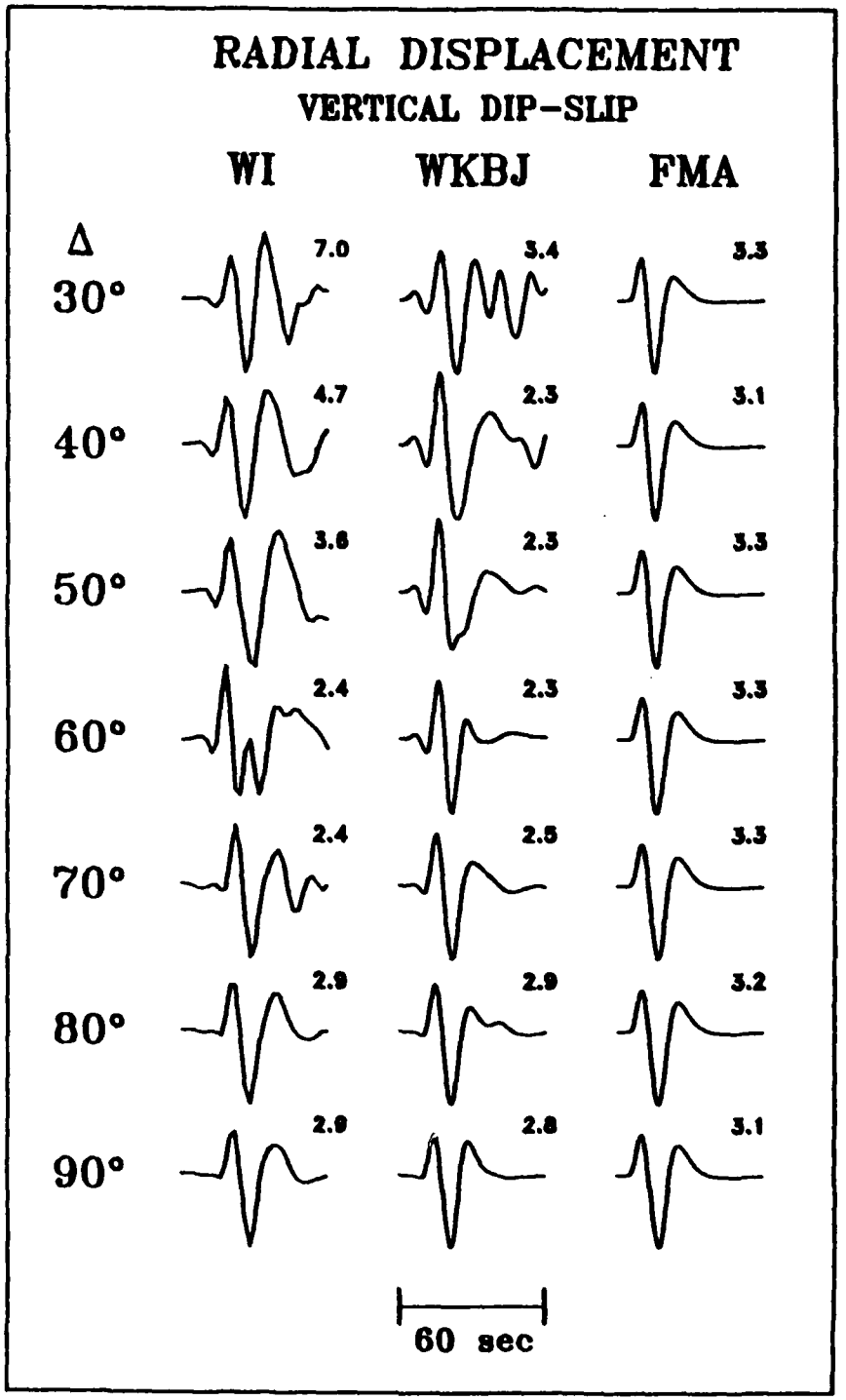
RADIAL DISPLACEMENT
VERTICAL DIP-SLIP
WI
WKBJ
FMA
Δ
30°
40°
50°
60°
70°
80°
90°
7.0
4.7
3.6
2.4
2.4
2.9
2.9
3.4
2.3
2.3
2.3
2.5
2.9
2.8
3.3
3.1
3.3
3.3
3.3
3.2
3.1
60 sec

FIG. 3b

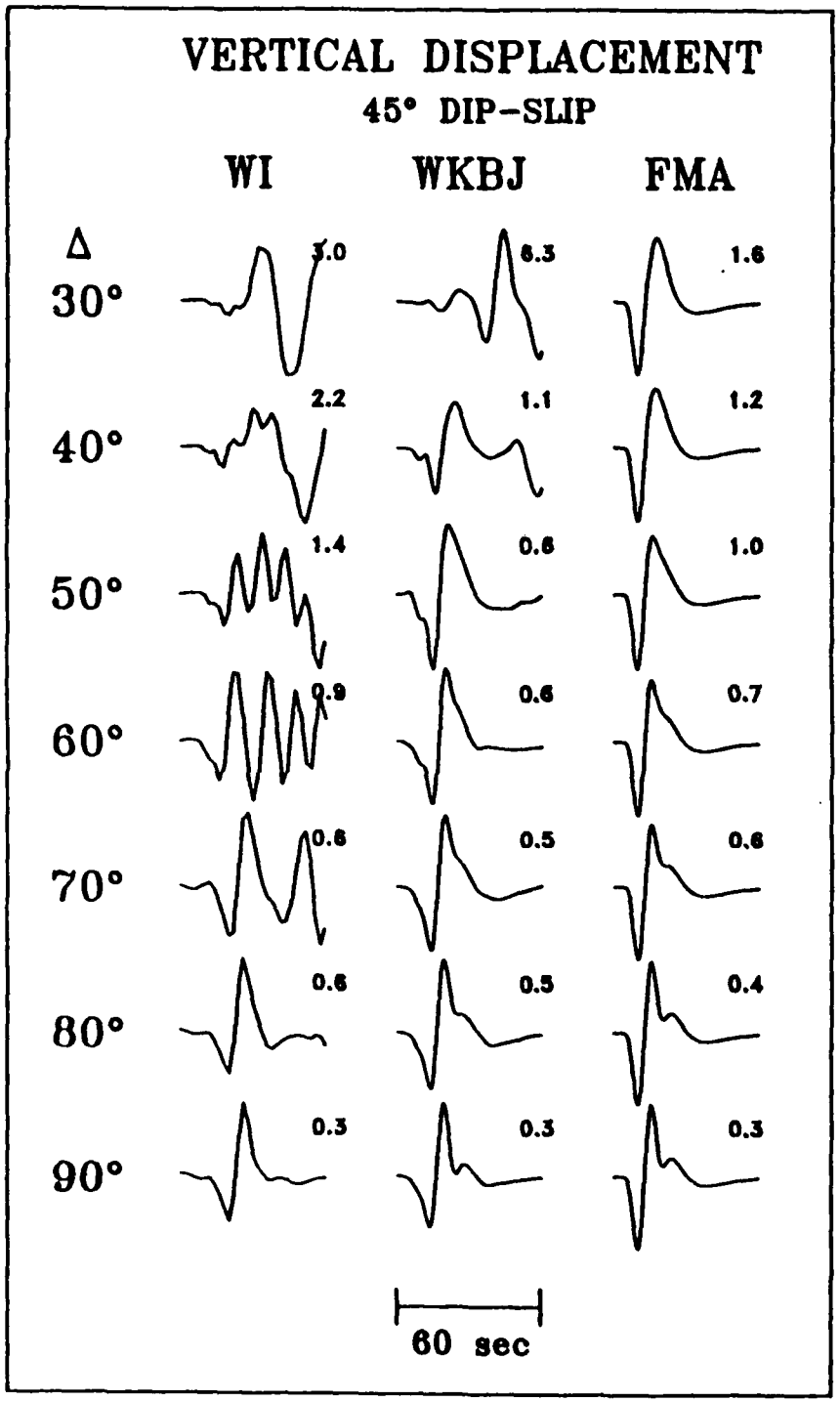
VERTICAL DISPLACEMENT
45° DIP-SLIP
WI
WKBJ
FMA
Δ
30°
40°
50°
60°
70°
80°
90°
3.0
6.3
1.6
2.2
1.1
1.2
1.4
0.8
1.0
0.9
0.6
0.7
0.6
0.5
0.6
0.6
0.5
0.4
0.3
0.3
0.3
60 sec

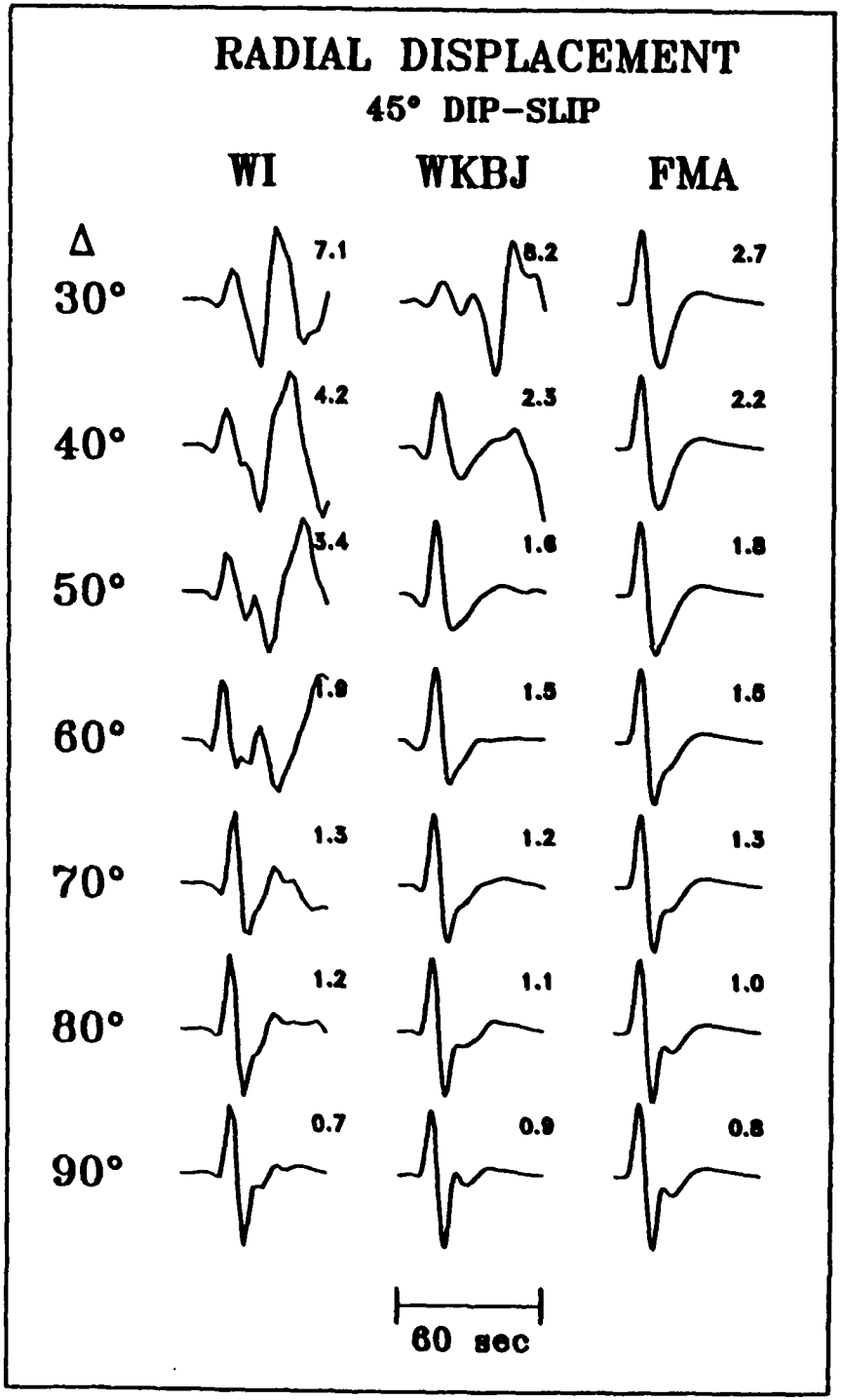
RADIAL DISPLACEMENT
45° DIP-SLIP
WI
WKBJ
FMA
Δ
30°
40°
50°
60°
70°
80°
90°
7.1
8.2
2.7
4.2
2.5
2.2
3.4
1.6
1.8
1.9
1.5
1.6
1.3
1.2
1.3
1.2
1.1
1.0
0.7
0.9
0.8
60 sec

Fig. 3C

Diffracted Sp generated under the Australian Shield

by Chang-Eob Baag

and

Charles A. Langston

Department of Geosciences

The Pennsylvania State University

University Park, PA 16802

April 18, 1985

Abstract

Diffracted Sp is found to be generated under the Australian shield by deep-seated Tonga, Honshu, and Bonin events. This seismic phase is set up at the Moho as a P head-wave by a critically-incident upgoing SV wave at an epicentral distances of around 50 degrees. The simple source time history inferred from P or SH particle motion and the absence of source structure effects on SV wave forms from a deep source suggest a diffracted Sp wave for the explanation of distorted SV waves recorded at the Mundaring station. The polarity of this phase arriving immediately after direct SV indicates a P-type of wave, excluding the possibility of other types of S waves like ScS. Using a WKBJ spectral method for SV wave propagation, synthetic seismograms for the direct SV and diffracted Sp are computed. With some modification of of the P-velocity model by Mathur and the S-velocity model presented by Goncz & Cleary for the Australian shield, synthetics produce the distinctive interference between direct SV and diffracted Sp seen in the data. The arrival time difference between direct S and diffracted Sp is sensitive to the P-velocity of the upper mantle. Results of the analysis reveal a higher P-velocity structure of upper mantle in the southwestern shield than in the northwest. The analysis of teleseismic SV waveforms and the diffracted Sp phase is a new and useful technique for determining regional variations in upper mantle P velocity structure.

Introduction

In contrast with the relatively simple behavior of SH waves, interactions between SV waves from seismic sources and horizontal boundaries of the near-surface earth structure result in complicated waveforms in long-period seismograms recorded at teleseismic distances. These waves include direct SV, shear-coupled PL (SPL), the Sp phase and diffracted Sp waves. SPL (Oliver, 1961) and diffracted Sp waves generated by the energy conversion from the SV wave usually disturb the waveform of the direct SV wave, since arrival times of these waves are similar. The diffracted Sp sometimes takes a more important role in the waveform distortion, depending on circumstances of source parameters, velocity structures, and epicentral ranges.

Diffracted Sp is a wave initially set up at the Moho as a P head-wave by an incident SV from the mantle (Figure 1), but eventually it takes on the characteristics of a whispering gallery phase when the P structure of the upper mantle has a positive velocity gradient (Frazer, 1977; Baag and Langston, 1985a). If the P-velocity decreases sufficiently rapidly with depth, the wave is refracted downward. Frazer (1977) synthesized the Sp-diffraction and concluded that the upper mantle should have a P wave low velocity zone immediately below the Moho on the grounds that no diffracted Sp phases have been observed. However, if it is observed, the wave could be a good indicator of upper mantle P velocity structure. It is excited by an S wave with a different ray parameter from that of the direct S wave and is sensitive to the P-velocity of the upper mantle.

For a shallow source depth, the direct SV and diffracted SP

waves are easily obscured by SPL waves, since the amplitude of the SPL wave is very large due to the excitation of SPL by S-reverbrations in the near-source structure (Baag and Langston, 1985a). Therefore, deep-seated sources may be more appropriate for determining the existence and the inteference effect of the Sp-diffraction in observed SV waveforms.

In this paper, we will present observations of the Sp-diffraction recorded at Mundaring, Australia, excited by large deep earthquakes in the Beniof zones of the western Pacific. Using a WKBJ spectral method (Baag and Langston, 1985b) to compute synthetic seismograms, we show that the diffracted Sp phase can be very prominent in the data and cause severe distortions of the teleseismic SV waveform. Furthermore, the timing and relative amplitude of the diffracted Sp phase can be used to detect regional variations in upper mantle structure.

Wave form distortions of SV waves recorded at Mundaring

We collected body wave data recorded at the Mundaring seismic station(Figure 2) from deep-seated earthquakes ocurring at the Tonga, south Honshu, and Bonin seismic regions and with body wave magnitude greater than 5.8. The Mundaring station is located at the southwestern tip of the Australian continent. The western and central parts of the continent have a shield type of structure in contrast to the aseismic platform (Knopoff,1972) of the eastern part which could also be classified as having a "tectonic" velocity structure. Hypocentral information about the selected earthquakes is given in Table 1. All the epicentral distances are greater than 55 degrees being in the range of

possible detection of the Sp-diffraction. The expected horizontal paths of S and diffracted Sp waves from these events are shown in Figure 2. Possible diffracted Sp waves excited by the two Tonga events occur beneath the continental shelf and their path to the Mundaring station is confined to the southwestern part of the continent. On the other hand, possible diffracted Sp waves set up by the Bonin and two Honshu events pass through the northwestern Australian shield.

Shown in Figure 3 are the digitized and rotated S wave data recorded at Mundaring. Simple wave forms for SH waves imply that source mechanisms of the events are not complicated. Radial components of the SV waves also have simple waveforms. However, wave shapes of the vertical components appear distorted and are quite different from those of radial and tangential components.

Particle motion plots of the 66/3/17 event and 74/11/29 event SV waveforms (Figure 4) show that there must be large later arriving P waves in them. Although complicated by interference with the backswing of the long-period instrument response, the S waveforms are not rectilinearly polarized. Later motion occurs roughly at right angles to the initial SV motion. Moreover, these P waves are not likely to be S-to-P conversions or reverberations in the local receiver crust. It is seen that the particle motion of teleseismic P waves from these same events show virtually no P-to-S conversions or reverberations caused by crustal discontinuities under the station(Figure 5).

Using techniques outlined by Burdick and Langston(1977) and Langston(1977;1979) an attempt was made to simultaneously model the P and SV waveforms with just the effects of plane wave

conversions and reverberations in the local crust. This proved impossible since the radical layered or dipping crustal structure needed to produce large reverberations in the SV waveforms also produced comparable effects in the P waveforms.

The precursors to direct S waves in Figure 3 are Sp phases. The Sp phase is a P-type wave converted from the upgoing direct S wave at the Mohorovicic discontinuity and it arrives earlier than the direct S wave (Jordan and Frazer, 1975: Langston, 1977). An experimental computation for the effect of the Sp phase on the waveform distortion of the direct S shows almost no influence of this phase on much of the waveform. An example of the result will be given in a later figure.

SPL waves from deep sources may have moderate amplitudes at the epicentral distances 58-68 degrees and could differentially distort wave forms of vertical and radial components of direct S waves by the elliptical particle motion of SPL. However, by the normal dispersion character of SPL, high-frequency components of SPL, comparable to the frequency content of the direct S wave, lag in time far behind the direct S at these epicentral distances. Long-period components of the SPL wave with arrival times close to direct S can be easily distinguished by wave length, and have small influence on the waveform distortion. Therefore, the main source of the disturbance in the SV waveform is not the SPL wave.

The wave ScS cannot be a cause of wave-form distortion, since it arrives about 1 minute later than the direct S even at the epicentral distance of 70 degrees; the two waves are separated enough to be distinguished. The horizontal polarization of ScS

particle motion is also inconsistent with the mainly vertical motion of later arrivals in the SV waveform.

Diffracted Sp satisfies the characteristic features of the disturbing wave. It is a P-type of wave, and its arrival time is close to, but after the direct S. We compute synthetic seismograms of SV waves including the diffracted Sp for these events in order to prove quantitatively that the disturbing waves in the data are from the Sp diffraction.

Synthetic seismograms

The WKBJ spectral method (Baag and Langston, 1985) is used for synthetic seismogram computations of SV waves including the diffracted Sp. The method employs WKBJ theory for a generalized ray in a vertically inhomogeneous halfspace and the propagator matrix method for waves in near-surface homogeneous layers. Wavenumber integration is done along the real axis of the wavenumber plane and anelasticity is included by using complex-valued velocity in all regions of the earth model.

The phase change due to the anelastic attenuation is included by using complex-valued velocity with the phase term

$$\frac{1}{v_e(z)} = \frac{1}{v(z)} \left[1 - \frac{i}{2Q(z)} - \frac{\ln(\gamma\omega/\omega_0)}{\pi Q(z)} \right]$$

where V_e, V, Q are effective velocity, wave velocity, and seismic quality factor, respectively. γ is the Euler-Masheroni constant and ω_0 is the cut-off frequency(Futterman, 1962). After computing the complex vertical phase time τ and the WKBJ potentials using the first two terms of the above equation as an effective

velocity, the potential of each WKBJ ray is multiplied by the phase term of the Q operator $\exp\left[i\omega t^* \ln(\gamma\omega/\omega_o)\right]$, where $t^* = 2\left|\mathrm{Im}(\tau)\right|$. This is a modification of the treatment of Q in the method of Baag and Langston(1985b).

The initial earth model of the crust and upper mantle down to the 200 km depth was compiled from the P-wave velocity structure of Mathur(1974) which is based on seismic refraction studies of southwestern Australia, and from the S-wave velocity structure of Goncz and Cleary (1976) based on a Rayleigh wave dispersion study of the Australian continent. The extended SNA model (Baag and Langston, 1985a) compiled from SNA (Grand and Helmberger, 1984) and the Jefferey-Bullen-A earth model are used for the velocity below 200 km depth. The Q structure used is a modified SL8 model (Baag and Langston, 1985a) from the original SL8 Q structure by Anderson and Hart (1978).

Before the flat-earth transformation (Muller, 1977) is applied to the original spherical earth model, the near-surface structure is divided into layers, and the other part of the vertical structure below the stack of layers is finely sampled simulating a vertically inhomogeneous profile for WKBJ rays. The base of the deepest layer is put at 200 km in oder to include the whispering gallery effect of the diffracted Sp phase below the Moho and allowing multiple reflections in each layer.

All sources are assumed to be point sources. Focal orientations of the two Tonga events are from Isacks and Molnar (1971). For the other three events, the orientations were estimated using the single station method of Langston(1982). The allowable variations in the fault orientations were further

examined by perturbing source parameters in the construction of the SV wave synthetics. The final source orientations are given in Table 2.

Wavenumber integration is limited to a finite slowness p-window rather than wavenumber k-window in order to include generalized rays with particular angles of incidence. The p-window for computations is defined by the maximum and mininmum ray slowness corresponding to geometric rays with epicentral distances of 15 and 80 degrees, respectively. This window scheme is wide enough to include the Sp-diffraction and SPL waves in addition to direct S waves. It is also wide enough to cover cosine tapers applied to both ends of the window for preventing non-physical diffraction caused by the truncation effect. Details of computational procedures in the wavenumber integration are given by Baag and Langston (1985a;b). In most calculations for synthetics 64 frequency points are used with time increament of 2 seconds. The far-field source time function of each event is approximated by a trapezoid with rise, constant level, and fall-off times of 1, 3, and 1 seconds, respectively. Ground displacement is convolved with the WWSSN 15-100 instrument response for Mundaring station.

By trial-and-error, the upper 200 km of the velocity structure was perturbed and synthetic seismograms were computed for the SV waveform data of Figure 3. The primary features of the waveforms of interest were the relative arrival time and amplitude of the Sp diffraction with respect to the direct SV wave. A cursory examination of the data shows that the Sp diffraction is significantly delayed in time for the events in

northern azimuths relative to the Sp diffraction set up by events to the east. This accounts for the compact waveforms of the Tonga events compared to the waveforms from the Honshu events. It was found that the average P velocity of the uppermost mantle primarily affected the Sp diffraction - S differential time. Thus, the final models shown in Figure 6 primarily reflect this fact. The deduced upper mantle structure from the data from eastern events (SWA) show slightly higher overall P velocities compared to structure deduced from the northern event data (NWA). It was also found that the amplitude of the Sp diffraction was not a sensitive function of details of the P velocity gradient in the upper mantle.

SV waves at several ranges for the south-western shield model, SWA, are computed for the Tonga 66/3/17 event to demonstrate the wave shape changes and the arrival time variations relative to direct S waves(Figure 7). This plot scheme makes it easy to identify the Sp-diffraction phase among the other seismic phases. In both the radial and vertical components appear Sp, direct S, diffracted Sp, and SPL waves in the order of arrival time. The diffracted Sp is close to the direct S at the epicentral distance of 52 degrees, and gradually separates from it with increasing distance. However, it is not completely separated even at 70 degrees due to high P-velocity at the Moho in the SWA model. It is seen that waveforms of the vertical components are more disturbed by diffracted Sp waves than those of radial components, which is in accordance with observations. The syntnetic waveform for the epicentral range of 58 degrees in Figure 7 corresponds to the observed source

distance.

Figure 8 shows synthetics for the direct S and the Sp precursor computed using ray theory. Also shown are the data waveforms and synthetics computed using the WKBJ spectral method. The ray synthetic shows only the Sp and S phases; the majority of the waveforms showing direct S. The WKBJ synthetics demonstrates that the Sp diffraction arrives soon after S, at this range, and severely distorts the vertical waveform relative to the ray result and in accordance with the data.

The focal orientations for the Honshu and Bonin events computed using the single station method present both a problem and an opportunity since the orientations are less accurately known compared to the Tonga events. Since the single station method only employed P, radial SV and tangential SH polarities and relative amplitudes, parameters for allowable mechanisms vary by 37 in strike, 27 in rake, and 83 degrees in dip for these events. Fortunately the waveform is not changed much by small rotations of the source orientation as long as geometrical rays are not near to the nodal line of the SV wave, even though absolute amplitudes may vary considerably. However, if the source is oriented such that the geometrical ray of direct S is near the SV nodal line than are rays exciting diffracted Sp, waveforms are drastically changed due to the relatively large amplitudes of the diffracted Sp compared to the direct S wave. It was seen that plausible variations of the mechanism for the Honshu 74/11/29 event accounted for the significant change in waveform compared to the other events. Figure 9 shows the variation of SV waveform with orientation parameters and

Figure 10 displays the waveform fit for each event.

In Figure 10, synthetics for the two Tonga events are computed using the SWA velocity model for the southwestern Australian shield (Figure 6), and those for Bonin and two Honshu events are computed using the northwestern shield model, NWA. Since the upper mantle P-velocity of the northwestern shield is smaller than that of the south-western shield, central swings in the vertical components of the S waves of the Bonin and two Honshu events become broader than those of two Tonga events due to the arrival time delay of the Sp-diffraction.

Discussion

We deduced from the characteristic features of the observed SV waves at Mundaring that the origin of the distortion of the teleseismic SV waveforms from deep sources is not the Sp, SPL, or ScS phases. We found from the comparison of data with synthetic seismograms that the diffracted Sp wave can explain most features of the SV waveform. Diffracted Sp satisfies the observed conditions for the disturbing wave: a large P wave arrival occurring after direct SV seen best in the vertical component with the proper arrival time, polarity and amplitude.

Since the Sp-diffraction is sensitive to the upper mantle P-velocity, its relative arrival time compared to direct S gives good constraint to the average P-velocity structure. The paths of the Sp-diffraction from events occurring to the east and north are different and are seen to have two somewhat different P velocity structures. The results show the P-velocity and its gradient with depth in the south-western region are larger than

those in the north-western region, even though both of the regions reflect a shield type of velocity structure with high P-velocity. The arrival time of the diffracted Sp relative to the direct S is relatively insensitive to the S-velocity structure of the upper mantle, since direct rays are near-vertical in incidence angle. An increase in the S velocity would decrease the S and diffracted Sp travel times by nearly the same amount. Therefore, there may be some ambiguity in S-velocities in the velocity model used here. It is possible that the S-velocity of the upper mantle in the south-western region may be larger than that in the north-western region if it is assumed that both regions have similar Poisson ratios. The same S-velocity model was used in computing the synthetic seismograms for both SWA and NWA models.

According to Ringwood's(1962a;b) continental evolution model deduced from heat-flow observations in the shield, concentrations of radioactive elements move upward in the formation of continental crust through partial melting and metamorphism. The removal of radionucleides by continuous erosion on the surface results in low heat flow in the crust and upper mantle. High seismic velocities in the upper mantle of the shield structure may be from this low temperature effect. Assuming this model, it may be inferred that the southwestern region is depleted in radioactive elements compared to the northwestern region. The regional heat-flow data (Cull and Denham, 1979) support this interpretation where it is seen that the Sp diffraction phase from Tonga events traverses an area of very low heat-flow(~30 mW/m^2). The Sp diffraction from events near Japan traverses an

area of slightly higher heat flow, ~40 mW/m^2, in agreement with the slightly lower mantle P velocities found for this line.

The high S-velocity of the crust in the velocity model (Figure 6) gives rise to a small amplitude Sp phase in the synthetic seismograms (Figures 8 and 10), which is appropriate if precursors to the direct S waves in the data from the Tonga 67/10/9 and Honshu 74/2/22 events (Figure 3 and 10) are not the Sp phase but some other effect of signal-generated noise. The velocities 3.7 and 4.0 km/sec could be reduced to 3.6 km/sec in order to produce a larger amplitude Sp phase. However, this does not affect the later arriving Sp-diffraction and its sensitivity to upper mantle P velocity.

The take-off angle of the direct S ray at the source to reach a station at 65 degrees differs from the angles of rays exciting the diffracted Sp by only about 6 degrees, assuming that the excitation occurs at 50 degrees. Therefore, the pattern of the wave-form distortion is not usually sensitive to the source orientation, even though the absolute amplitude of the waves can change. However, if the station is located near to the SV nodal line the relative amplitude of the diffracted Sp becomes very large as seen in the Honshu 74/11/29 event. This could be useful in the inversion of dislocation source orientation using synthetic seismograms provided the receiver crustal structure and regional mantle structure is reasonably well known.

Finally, this study demonstrates the utility of modeling the complexities of teleseismic SV waves in determining regional mantle structure. The diffracted Sp phase allows, in a sense, for refraction profiles to be constructed in otherwise

inaccessible regions. Observations of these waves at a few stations and at a number of azimuths gives a relatively fast and inexpensive look at mantle P velocity structure and its lateral variations. Analysis of teleseismic SV waves should provide new and useful constraints in future velocity structure studies.

Conclusions

The SV waveform at teleseismic distance is influenced by complex P wave propagation effects. We have shown that even at distances of 68 degrees from the source, the direct SV wave is contaminated by the Sp diffraction which propagates in the upper mantle after being set up at distances of around 50 degrees.

At the Mundaring station in southwest Australia the Sp diffraction excited by deep-seated earthquakes is very large and significantly distorts the observed SV waveforms. Modeling the SV waveforms with a WKBJ spectral method results in the ability to resolve the difference in average mantle P wave velocity along azimuths north and east of the station. The timing of the diffracted Sp phase relative to direct SV suggests that mantle P velocity is higher in southwestern Australia than in northwestern Australia, in agreement with interpretations of observed heat-flow data.

The teleseismic SV waveform appears to be a useful new source of data for examining upper mantle P velocity structure and its regional variations.

Acknowlegements

This research was supported by the Advanced Research Projects Agency of the Department of Defense and was monitored by the Air Force Office of Scientific Research under Contract #F49620-83-K-0019.

References

Anderson, D.L and R.S. Hart (1978). Q of the earth, Jour. Geophys. Res., 83, 5869-5882.

Baag, Chang-Eob and C.A. Langston (1985a). Shear coupled PL, Geophys. Jour. Roy. astr. Soc.,80,363-386.

Baag, Chang-Eob and C.A. Langston (1985b). A WKBJ spectral method for computation of SV synthetic seismograms in a cylindrically symetric medium, Geophy. Jour. Roy. astr. Soc., 80,387-418.

Burdick, L.J. and C.A. Langston (1977). Modeling crustal structure through the use of converted phases in teleseismic body waveforms, Bull. Seism. Soc. Am., 67, 677-692.

Cull, J.P. and D. Denham (1979). Regional variations in Australian heat flow, B.M.R. Journal of Australian Geology and Geophysics, 4, 1-13.

Dziewonski, A.M. (1971). On regional differencies in dispersion of mantle Rayleigh waves, Geophy. Jour. Roy. astr. Soc., 22, 289-325.

Frazer, N.L. (1977). Synthesis of Shear coupled PL. Ph.D. Thesis, Princeton University.

Futterman, W.I. (1962). Dispersion of body waves, Jour. Geophys. Res., 67, 5279-5291.

Goncz, J.H. and J.R. Cleary (1976). Velocities in the structure of the upper mantle beneath Australia, from Rayleigh wave observations, Geophys. Jour. Roy. astr. Soc., 44, 507-516.

Grand, S.P. and D.V. Helmberger (1984). Upper mantle shear structure of North America, Geophy. Jour. Roy. astr. Soc. 76, 399-438.

Isacks, B. and P. Molnar (1971). Distribution of stresses in the descending lithosphere from a global survey of focal-mechanism solutions of mantle earthquakes, Reviews of Geophysics and Space Physics, 9, 103-174.

Jordan, T.H. and N.L. Frazer (1975). Crustal and upper mantle structure from Sp phases, Jour. Geophy. Res., 80, 1504-1518.

Knopoff, L. (1972). Observation and inversion of surface-wave dispersion, Tectonophysics, 13, 497-519.

Langston, C.A. (1977). Corvallis, Oregon, crustal and upper mantle receiver structure from teleseismic P and S waves. Bull. Seism. Soc. Am., 67, 713-724.

Langston, C.A. (1979). Structure under Mount Rainier, Washington, inferred from teleseismic body waves. Jour. Geophys. Res., 84, 4749-4762.

Langston, C.A. (1982). Single-station fault-plane solutions, Bull. Seism. Soc. Am., 72, 729-744.

Mathur, S.P. (1974). Crustal structure in southwestern Australia from seismic and gravity data, Tectonophysics, 24, 151-182.

Muller, G. (1977). Earth-flattening approximation for body waves derived from geometric ray theory - improvement, corrections, and range of applicability, Jour. Geophys., 42, 429-436.

Oliver, J. (1961). On the long period character of shear waves,

Bull. Seism. Soc. Am., 51, 1-12.

Ringwood, A.E. (1962a). A model for the upper mantle, Jour. Geophys. Res., 67, 857-867.

Ringwood, A.E. (1962b). A model fro the upper mantle - 2, Jour. Geophy. Res., 67, 4473-4477.

Toksoz, N.M., M.A. Chinnery, and D.L. Anderson (1967). Inhomogeneities in the earth's mantle, Geophys. Jour., Roy. astr. soc., 13, 31-59.

Table 1. List of events

Event	Origin time	Location (degree)	Depth (km)	m_b
Tonga 1966/3/17	15h 50m 32.3s	21.1S 179.1W	630	5.9
Tonga 1967/10/9	17h 21m 46.2s	21.1S 179.2W	605	6.2
Bonin 1968/10/7	19h 20m 20.8s	26.3N 140.7E	518	6.1
Honshu 1974/11/29	22h 05m 23.5s	30.7N 138.4E	429	6.1
Honshu 1974/2/22	00h 36m 54.6s	33.2N 137.0E	391	5.9

Table 2. Source orientations

Event	Orientation (Deg)		
	strike	dip	rake
Tonga 1966/3/17	34.	70.	-85.
Tonga 1967/10/9	55.	86.	-84.
Bonin 1968/10/7	110.	50.	280.
Honshu 1974/11/29	150.	10.	245.
Honshu 1974/2/22	10.	50.	140.

Figure Captions

Figure 1: Schematic diagram for the generation of diffracted Sp.

Figure 2: Horizontal paths of S and diffracted Sp waves. Filled star, triangle, and circle indicate locations of epicenter, Mundaring station and the approximate position of the Sp diffraction excitation, respectively.

Figure 3: S wave data recorded at Mundaring station showing distorted waveforms.

Figure 4(a): Particle motion of SV waves from the Tonga 66/3/17 event. The motion plot of the earlier portion of the seismogram has mainly direct S. P-type motion is shown in the right hand plot although the instrumental backswing from the direct S wave distorts its expected rectilinear polarization.

Figure 4(b): Particle motion of SV waves from Honshu 74/11/29 event. Same scheme as 4(a).

Figure 5: Waveforms of P wave data recorded at Mundaring.

Figure 6: Velocity structures deduced by the trial-and-error method, using the comparison of synthetic seismograms with the data. VP and VS are velocities of the P and S waves. respectively. NWA and SWA indicate P velocity models for northwestern and southwestern Australia. Even though velocities down to 300 km are shown, actual velocities used in computations continue through the lower mantle.

Figure 7: Synthetic SV waves at several ranges for the Tonga

66/3/17 event.

Figure 8: Synthetics of the SV waveform computed using ray theory and by the WKBJ spectral methods compared with data of the Tonga 66/3/17 event.

Figure 9: Variation of the SV waveform with change of the dislocation source orientation for the Honshu 74/11/29 event. In the order of increasing ID number, the angles of dip and rake are (5,245), (5,250), (5,255), (10,245), (10,250), (10,255), (15,245), (15,250), (15,255) degrees, respectively. The strike angle is the same in all cases, and is 150 degrees.

Figure 10: Comparison of synthetic SV and data waveforms of all events. The SWA velocity model (Figure 6) is used for the two Tonga events, and the NWA velocity model is used for the Bonin and two Honshu events.

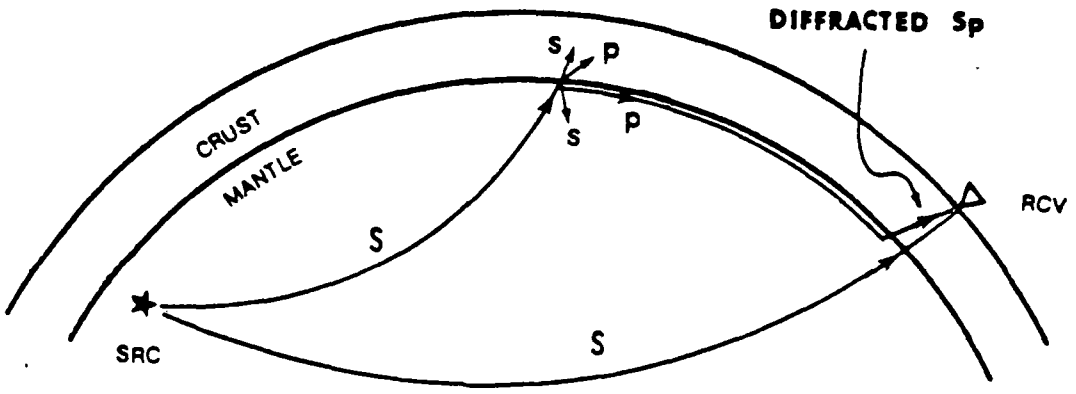

Fig. 1

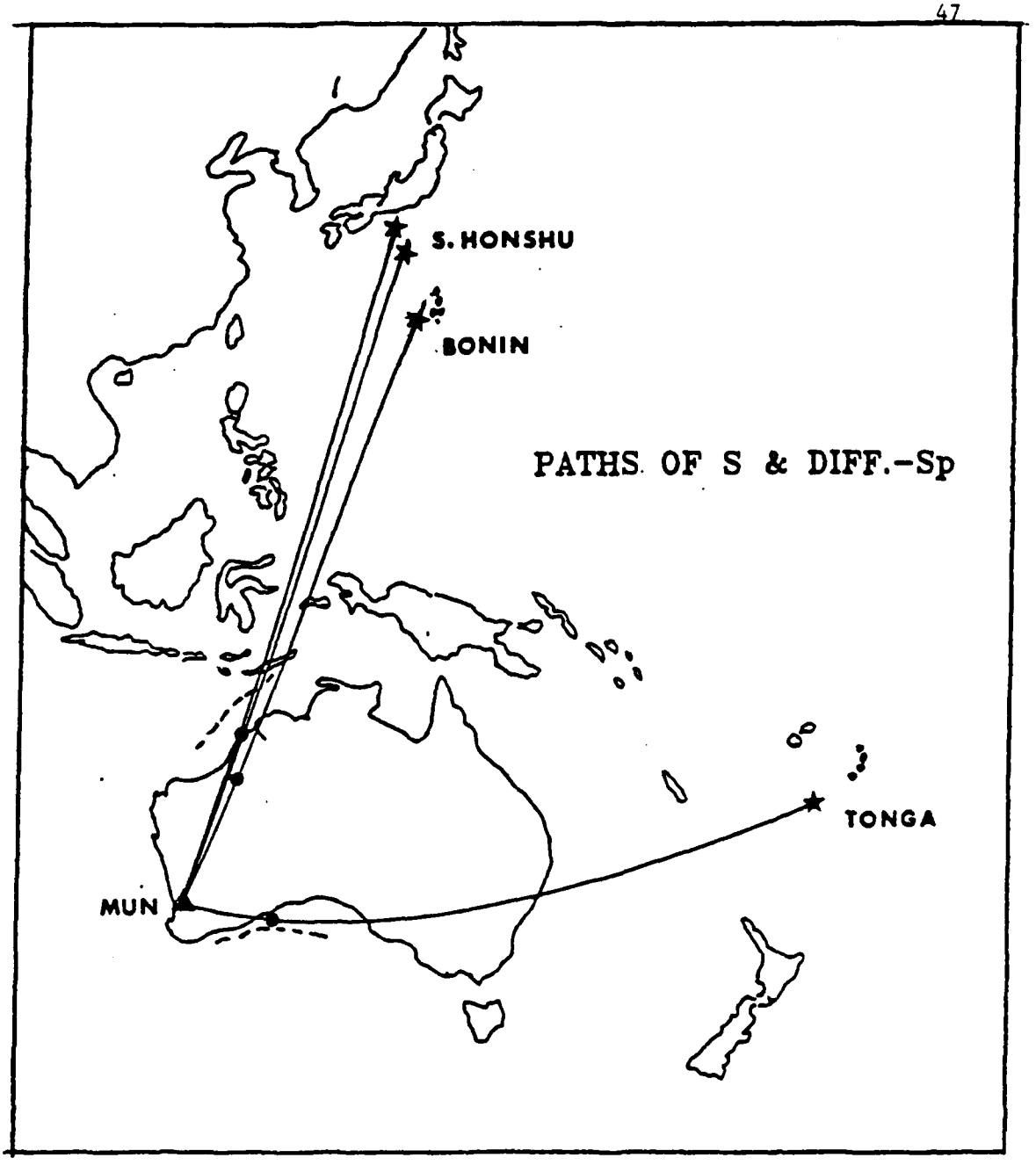

Fig. 2

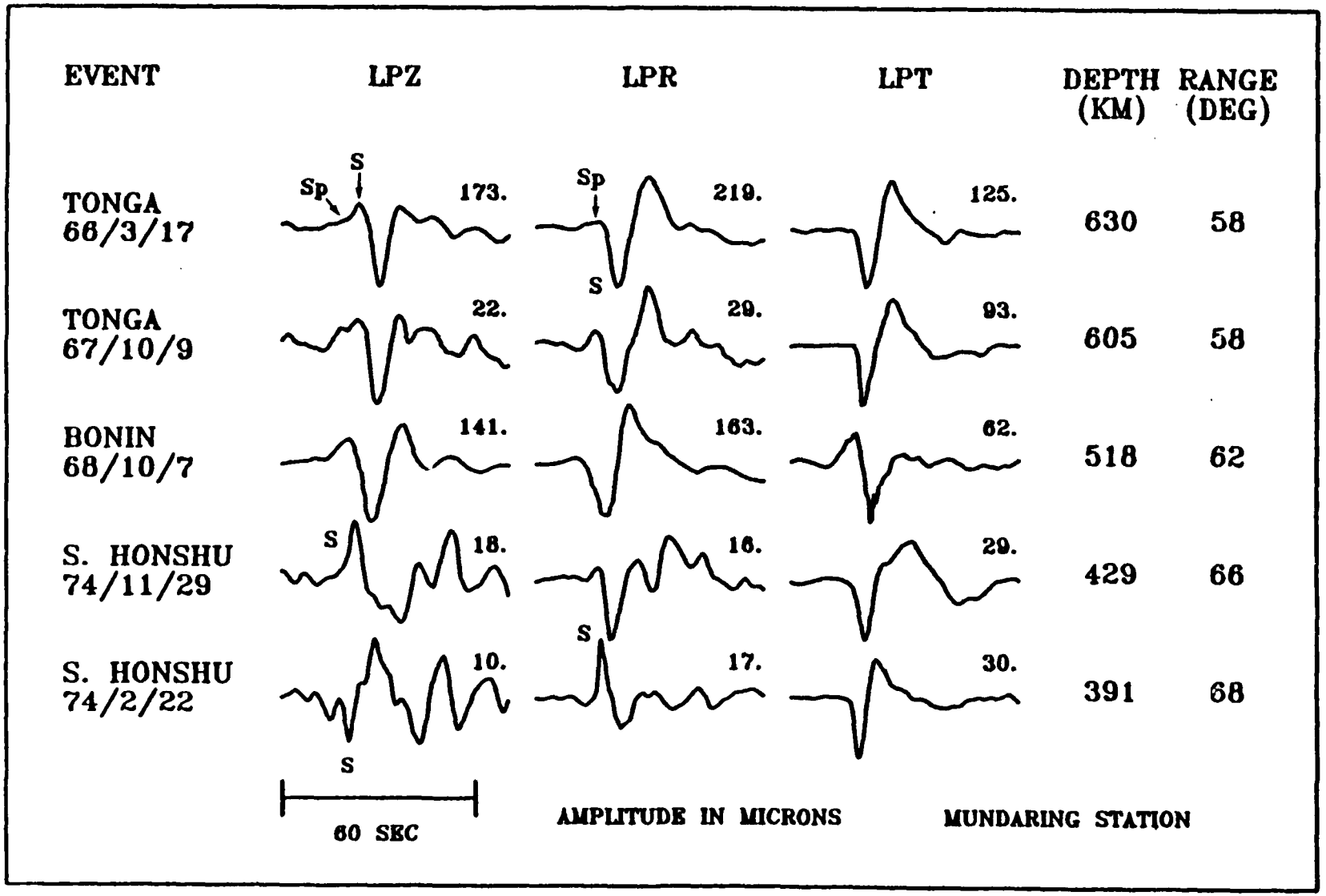
EVENT
LPZ
LPR
LPT
DEPTH (KM)
RANGE (DEG)
TONGA 66/3/17
Sp
S
173.
Sp
219.
125.
630
58
TONGA 67/10/9
S
22.
29.
93.
605
58
BONIN 68/10/7
141.
163.
62.
518
62
S. HONSHU 74/11/29
S
18.
16.
29.
429
66
S. HONSHU 74/2/22
S
10.
S
17.
30.
391
68
S
60 SEC
AMPLITUDE IN MICRONS
MUNDARING STATION

Fig 3

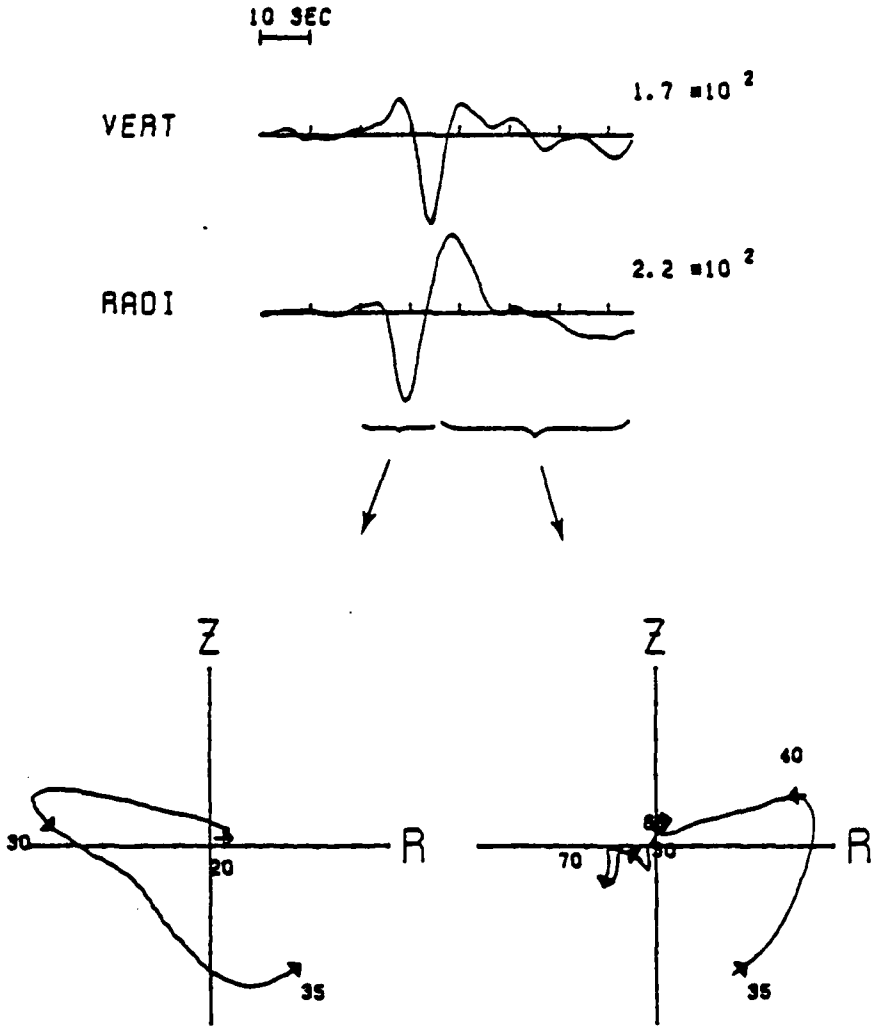

Fig 4(a)

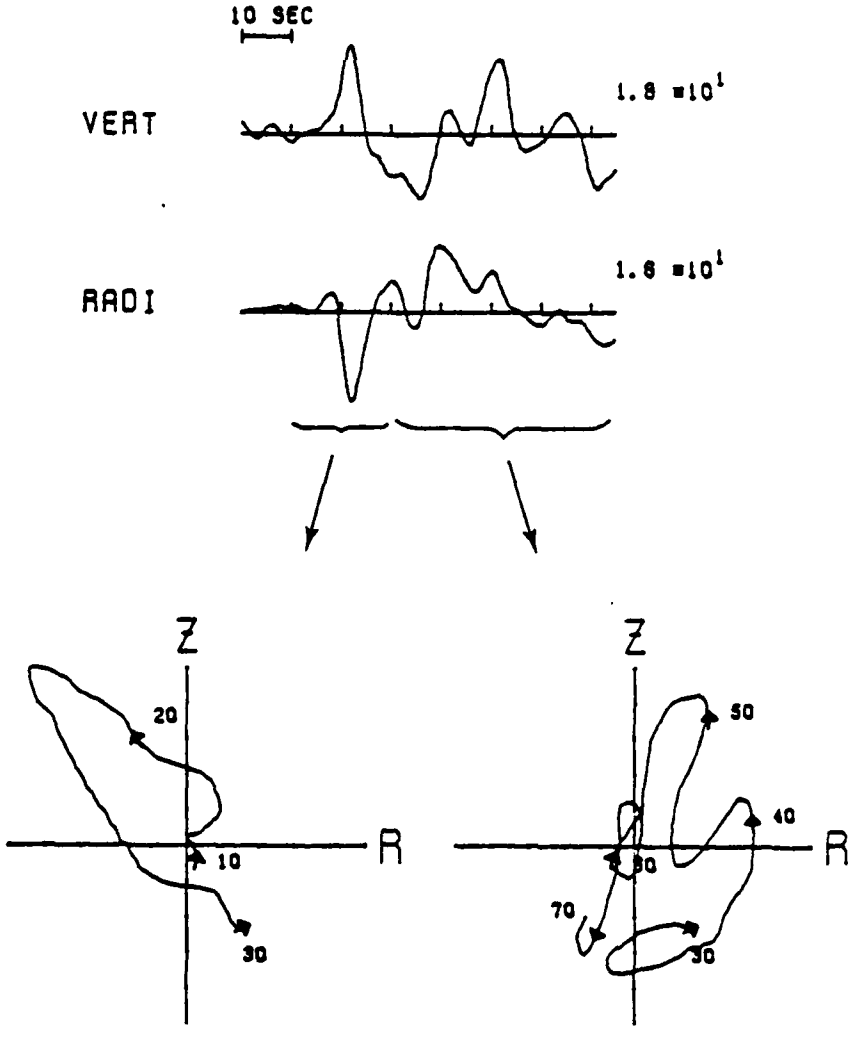

Fig 4(b)

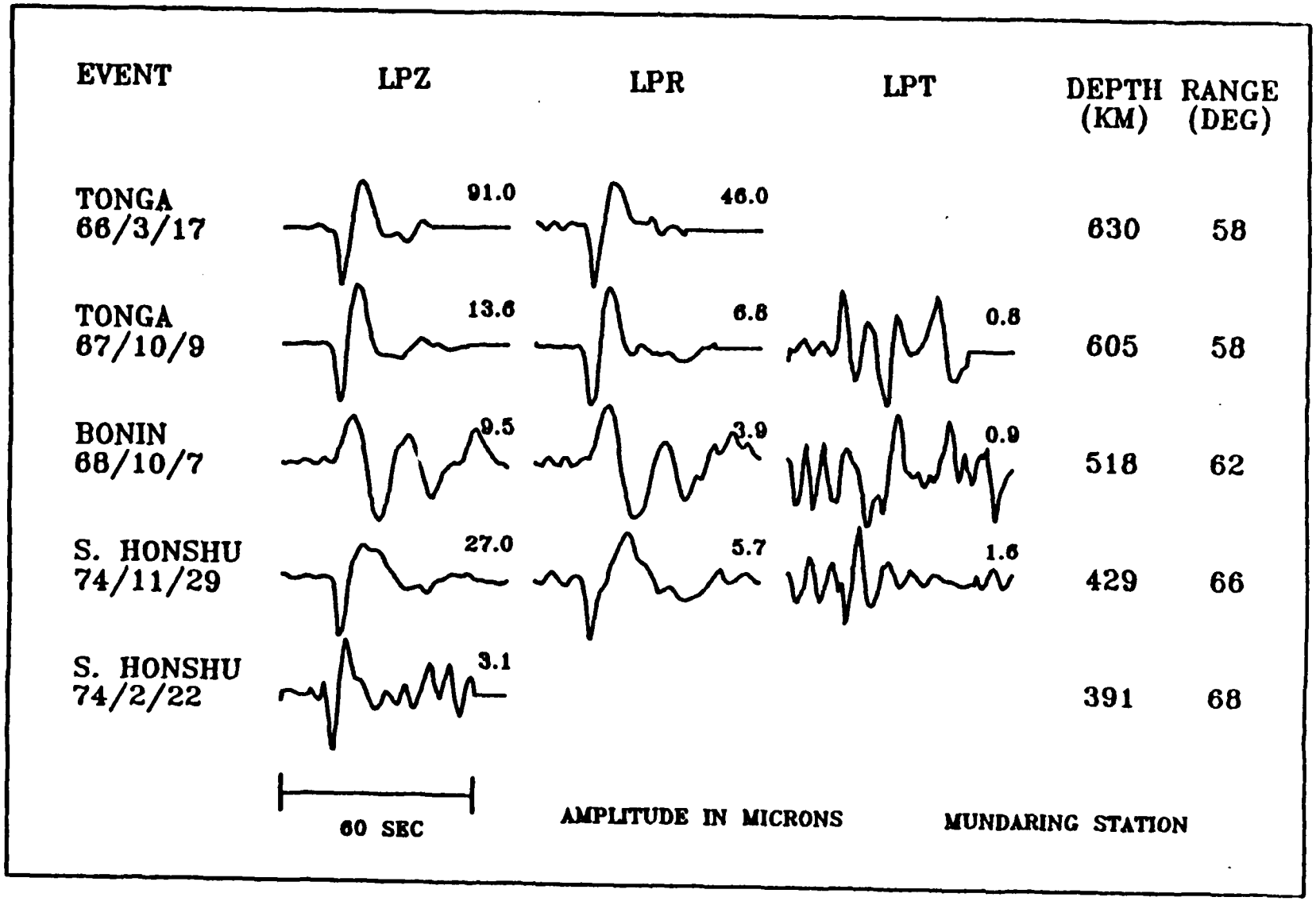
EVENT
LPZ
LPR
LPT
DEPTH (KM)
RANGE (DEG)
TONGA 66/3/17
91.0
46.0
630
58
TONGA 67/10/9
13.6
6.8
0.8
605
58
BONIN 68/10/7
9.5
3.9
0.9
518
62
S. HONSHU 74/11/29
27.0
5.7
1.6
429
66
S. HONSHU 74/2/22
3.1
391
68
60 SEC
AMPLITUDE IN MICRONS
MUNDARING STATION

Fig. 5

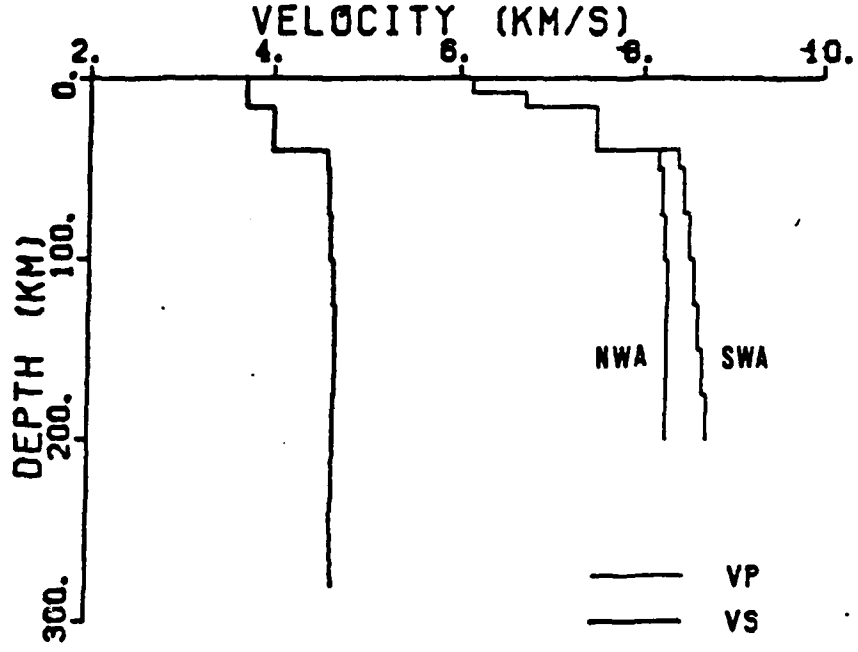

Fig. 6

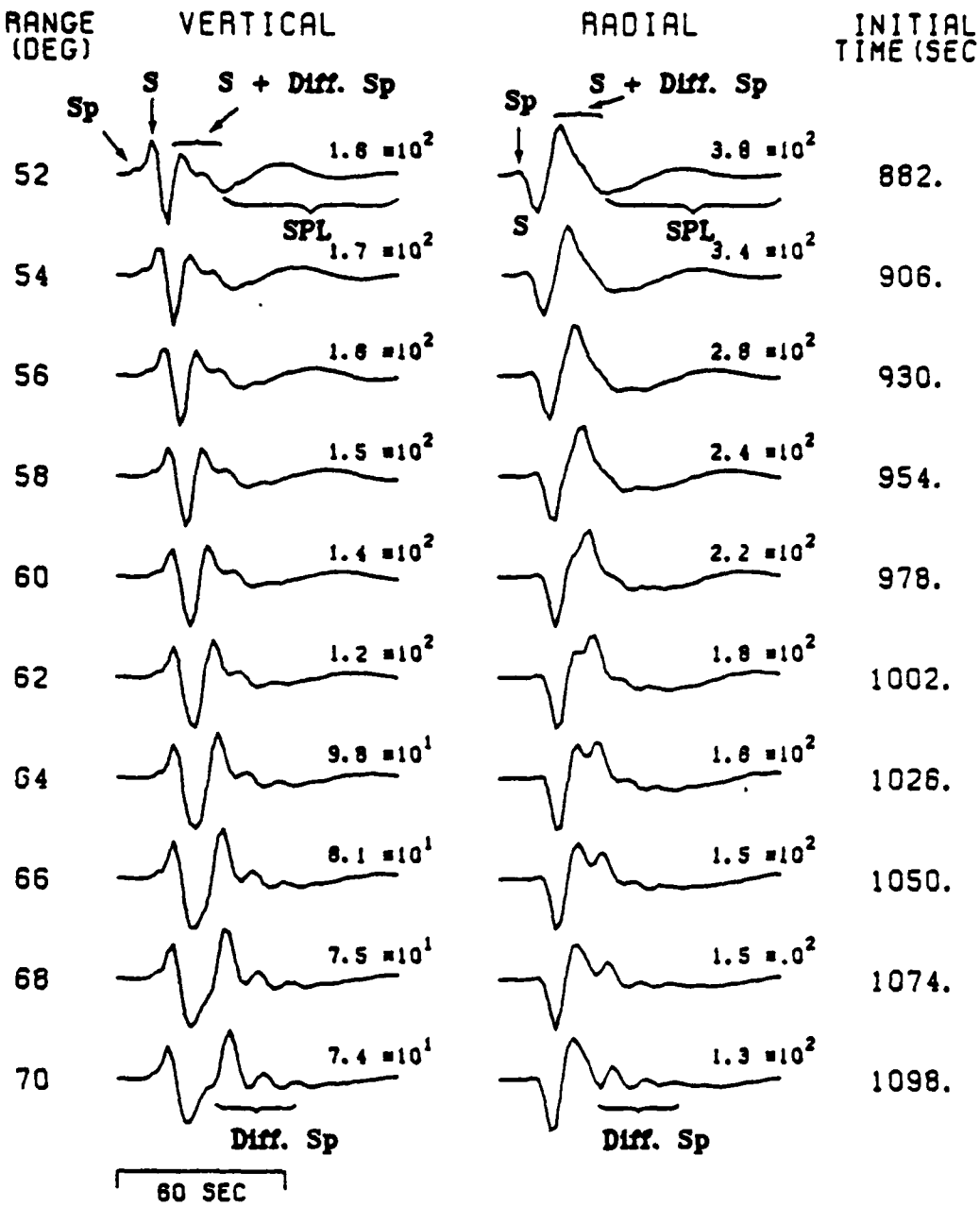
RANGE (DEG)
VERTICAL
RADIAL
INITIAL TIME (SEC)
Sp
S
S + Diff. Sp
SPL
Diff. Sp
60 SEC
52
54
56
58
60
62
64
66
68
70
1.6 ×10²
1.7 ×10²
1.6 ×10²
1.5 ×10²
1.4 ×10²
1.2 ×10²
9.8 ×10¹
8.1 ×10¹
7.5 ×10¹
7.4 ×10¹
3.8 ×10²
3.4 ×10²
2.8 ×10²
2.4 ×10²
2.2 ×10²
1.8 ×10²
1.6 ×10²
1.5 ×10²
1.5 ×.0²
1.3 ×10²
882.
906.
930.
954.
978.
1002.
1026.
1050.
1074.
1098.

Fig 7

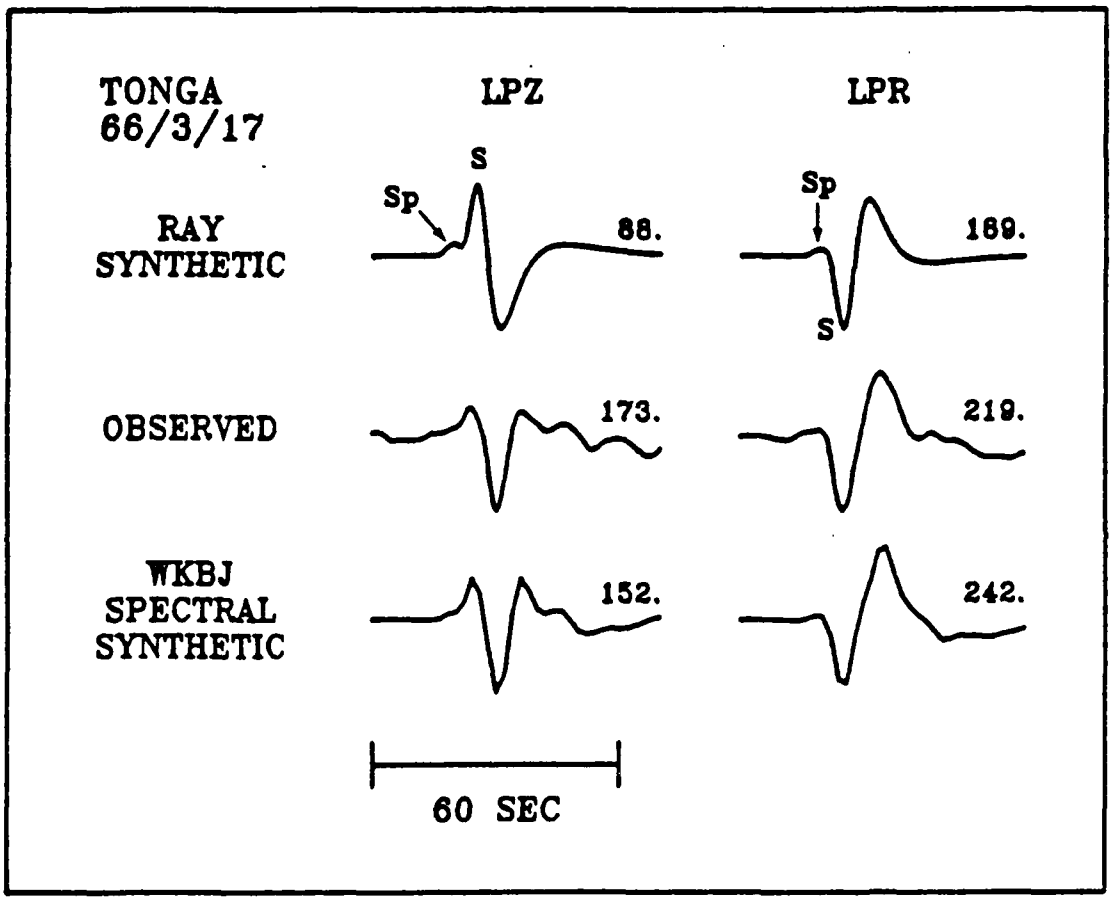
TONGA
66/3/17
LPZ
LPR
S
Sp
Sp
S
RAY
SYNTHETIC
88.
169.
OBSERVED
173.
219.
WKBJ
SPECTRAL
SYNTHETIC
152.
242.
60 SEC

Fig 8

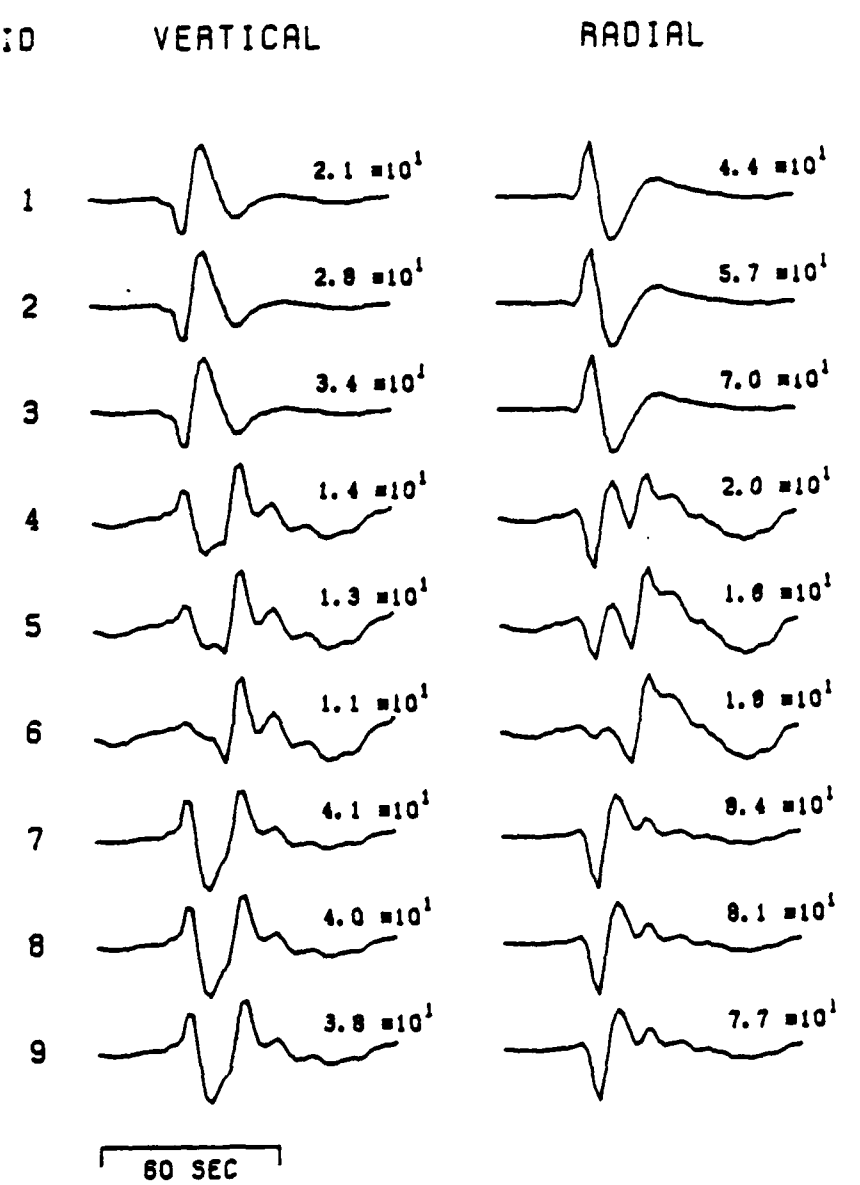
ID
VERTICAL
RADIAL
1
2.1 ×10¹
4.4 ×10¹
2
2.8 ×10¹
5.7 ×10¹
3
3.4 ×10¹
7.0 ×10¹
4
1.4 ×10¹
2.0 ×10¹
5
1.3 ×10¹
1.6 ×10¹
6
1.1 ×10¹
1.8 ×10¹
7
4.1 ×10¹
8.4 ×10¹
8
4.0 ×10¹
8.1 ×10¹
9
3.8 ×10¹
7.7 ×10¹
60 SEC

Fig 9.

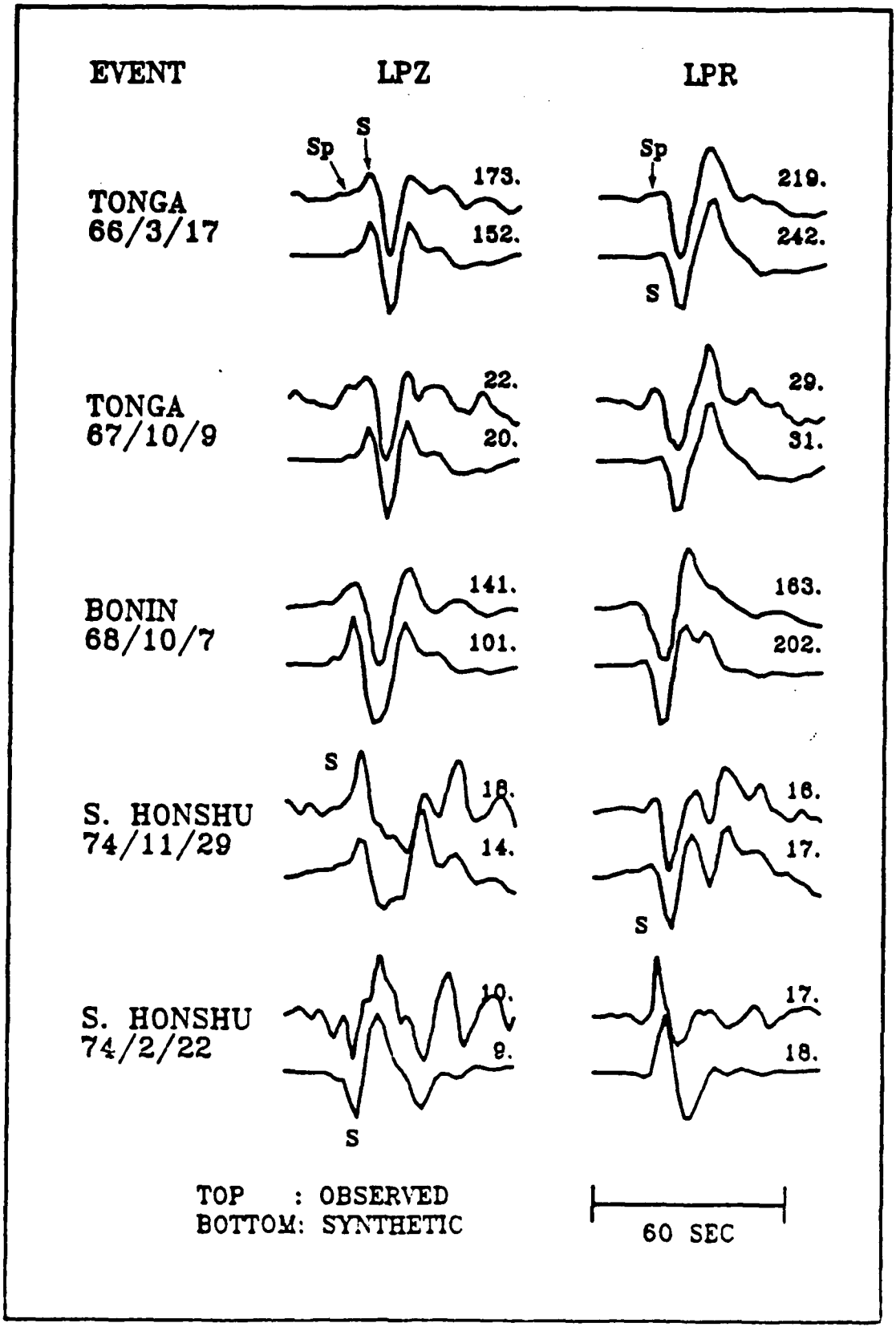
EVENT
LPZ
LPR
TONGA
66/3/17
Sp
S
173.
152.
Sp
219.
242.
S
TONGA
67/10/9
22.
20.
29.
31.
BONIN
68/10/7
141.
101.
163.
202.
S. HONSHU
74/11/29
S
18.
14.
16.
17.
S
S. HONSHU
74/2/22
10.
9.
17.
18.
S
TOP : OBSERVED
BOTTOM: SYNTHETIC
60 SEC

Fig. 10

The Pennsylvania State University

The Graduate School

Geosciences Department

Upper Mantle P Velocity Structure of Eastern North America: Model S8 and Data from the Hispaniola Earthquake of 14 September 1981

A Paper in

Geophysics

by

Nancy L. Niemann

Submitted in Partial Fulfillment
of the Requirements
for the Degree of

Master of Science

May 1985

ABSTRACT

Body-wave forms from the eastern Hispaniola earthquake of September 14, 1981, were compared to synthetic seismograms to investigate the upper mantle P velocity structure of eastern North America. The event occurred at an intermediate depth, 190 km, ensuring that phases that arrived after direct P were sufficiently delayed that they did not interfere with the triplicated direct P phases. Triplicated phases are best observed in intermediate-period data. The lower discontinuity lies at 670 km, instead of at 650 km as in a published model for the region. The new velocity model is identical to the published model above 640 km.

TABLE OF CONTENTS

LIST OF TABLES

LIST OF FIGURES

ACKNOWLEDGMENTS

I would like to express my gratitude to and admiration for Dr. Charles A. Langston, who proposed this study, provided the software that calculated synthetic seismograms, and advised me throughout my research. His insight, experience, and above all patience allowed the completion of this work.

To David Johnston go my warm thanks for making available his digitized records of the Hispaniola earthquake. Richard "Boomer" Baumstark at the Center for Seismic Studies, Washington DC, enabled my access to the RSCP data set.

Highest praises go to the Geosciences Department, and to Dr. Langston in particular, for procuring and maintaining the PRIME minicomputer, on which I made my calculations. I used the Geophysics Program's IBM PC to prepare this manuscript.

My research was partially supported by the Advanced Research Projects Agency and monitored by the Air Force Office of Scientific Research under Contract F49620-83-K-0019. The Geosciences Department provided additional support with teaching and research assistantships.

INTRODUCTION

Studies of seismic waveforms recorded at stations 15° to 30° from earthquake sources have produced as much knowledge about the methods used to study them as they have about the P and S velocities of the upper mantle. In the present study, an attempt to define a slight lateral variation in the position of the 650-km discontinuity beneath the eastern U. S. contributes to this knowledge.

The eastern Hispaniola earthquake of September 14, 1981, Mb=5.8, generated waveforms that, at upper mantle distances, are useful for studying wave propagation beneath the east coast of the U. S. The earthquake source function is simpler than many that have been modeled in previous upper mantle waveform studies (cf Burdick, 1981). The event's hypocenter was 190 km deep. Phases arriving after direct P are sufficiently delayed that they do not interfere with the triplicated P phases. In principle, therefore, the simpler source function and greater depth should make observing the triplication branches easier.

We attempt to interpret the P waveforms in the first 5 to 10 seconds of the upper mantle records by comparing them to synthetic seismograms calculated for Burdick's (1981) S8 model for an adjacent and overlapping region. Since S8 does not predict the Hispaniola travel times and waveforms well, we attempt to find a new model that will.

Helmberger and Wiggins (1971), began their upper mantle studies by inverting travel time data to derive a starting velocity model. They proceeded to manipulate the model by trial and error until waveforms calculated from it satisfied observed waveforms.

If a published velocity model exists, then inverting travel times is not necessary. The availability of model S8 obviates inverting travel time data to obtain a starting velocity model here. A number of authors have successfully manipulated published models derived by waveform analysis for regions that they were studying with more recently available data (Helmberger, 1973, Wiggins and Helmberger, 1973, Helmberger and Engen, 1974, Burdick and Helmberger, 1978, Given and Helmberger, 1980, Burdick, 1981, and Grand and Helmberger, 1984).

Burdick (1981) set out to demonstrate that variations in the upper mantle P velocity structure beneath North America are confined to the upper 250 km. He constructed two models, S8 for stable continental shield, and T9 for the tectonic region, that are identical below 250 km and different above. Given and Helmberger (1980) found that, below 250 km, "there is no distinguishable difference between the model proposed for northwestern Eurasia [their model] and models derived for the U. S." (p. 7183). Grand and Helmberger (1984) reached a similar conclusion about S velocities. Their models SNA for shield and TNA for tectonic

areas of North America differ only above 405 km. Cara's (1979) study of higher-mode Rayleigh waves suggests that the main variations in S velocity occur above 250 km.

Through trial and error inversion, we develop a velocity model that satisfies the Hispaniola data, and that is slightly different from S8. The new model, although otherwise identical to S8, has its lower velocity discontinuity at 670 km.

Since we do not use a formal inversion procedure to derive the new model as did Given (1984), we have no quantitative measure of its uniqueness or of its resolution in the vicinity of the 650-km discontinuity. We gain considerable insight into how unique our model is by applying the trial and error inversion technique itself. We interpret our model by referring to the results of Given's (1984) formal inversion of waveforms for upper mantle structure.

STUDY AREA

The Hispaniola earthquake of September 14, 1981, was recorded at stations in eastern North America at upper mantle distances (Figure 1). Naturally the character of the wave propagation paths from the source to each station will change with azimuth. To reduce problems with resolution and uniqueness, upper mantle velocity studies are traditionally conducted for geographic regions for which large numbers of upper mantle observations have accumulated. Furthermore, the least ambiguous solution to the inversion problem will result if the observations are as evenly and closely distributed as possible with distance. We must balance the advantages of working with a large data set against the disadvantage of averaging too large a region, since, the larger the area, the greater the chance of including regions of the upper mantle with slightly varying character.

Previous authors (Helmberger and Wiggins, 1971, Wiggins and Helmberger, 1973, Burdick, 1981) have found that describing the upper mantle data of North America requires two velocity models: one for the tectonic area to the west, and a second for the stable shield region. If the upper mantle beneath the stable continental shield region has little lateral variation, so that source-to-station wave propagation paths are similar, then one model should fit most of the data.

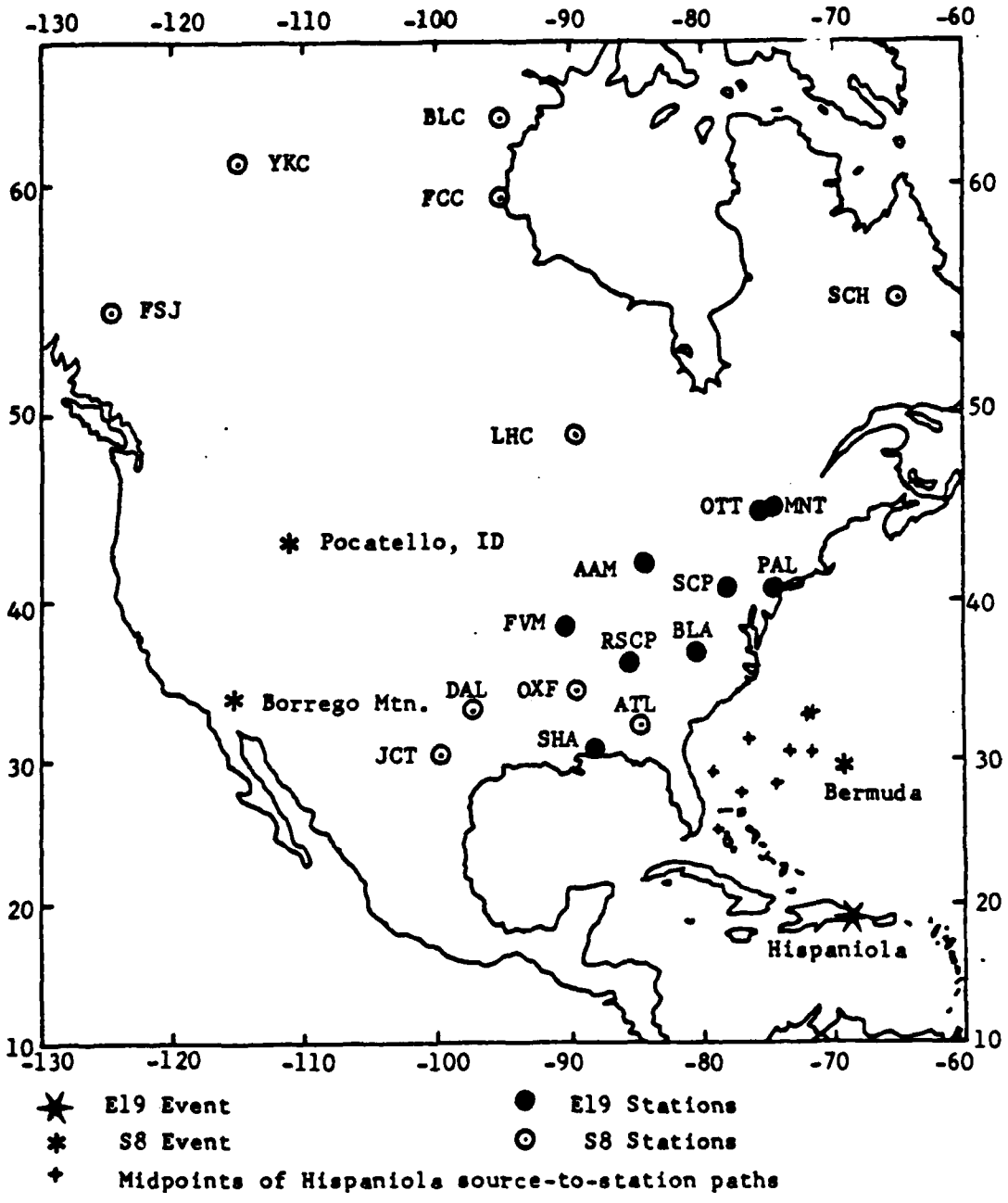

Figure 1. The locations of the eastern Hispaniola earthquake and WWSSN, RSTN, and Canadian network stations whose records were available for this study. Also shown are the events and stations used to derive S8. (Modified from Burdick, 1981.)

All of the North American stations at upper mantle distances from the Hispaniola event recorded waves that had traveled paths underneath first oceanic crust and then continental shelf and stable continental shield crust. Model S8 was developed from source-to-station ray paths that, in almost every case, sampled the upper mantle beneath stable continental areas. North American records of the 1978 Bermuda earthquake are a subset of this data set.. Like Hispaniola source-to-station paths, those from the Bermuda event are partly oceanic. Since the region covered by the Hispaniola stations overlaps the Bermuda region from the south, upper mantle wave propagation should be similar in both cases. Since the S8 model averages European and North American upper mantle data, however, it may not fit the Hispaniola data very well.

DATA SET

Figures 2a and 2b show the reduced travel time curves for P-wave rays from a source at 190 km depth for the S8 model and for our model E19. The distance ranges over which arrivals are triplicated by the presence of a velocity discontinuity are obvious. For example, at any particular source-to-station distance between 20° and 24°, the P waveform will be complicated by the interference of three P arrivals from near the 650-km discontinuity. This information aids in selecting North American stations that are at distances from the Hispaniola epicenter such that their records would be affected by upper mantle discontinuities.

Long-period vertical-component records from nine North American WWSSN and Canadian Seismograph Network stations at ranges less than 28° were available and of good quality. These photographic records were digitized at an irregular interval of one to three samples/second and then resampled at a constant interval of four samples/second.

Digital broad-band intermediate period records were available from two North American stations. RSCP (of the Regional Seismic Test Network) was sampled at four samples/sec. The DWWSSN station SCP, sampled at 10 samples/sec, proved to be the single most useful data record available to this study. With proper adjustments to the S8

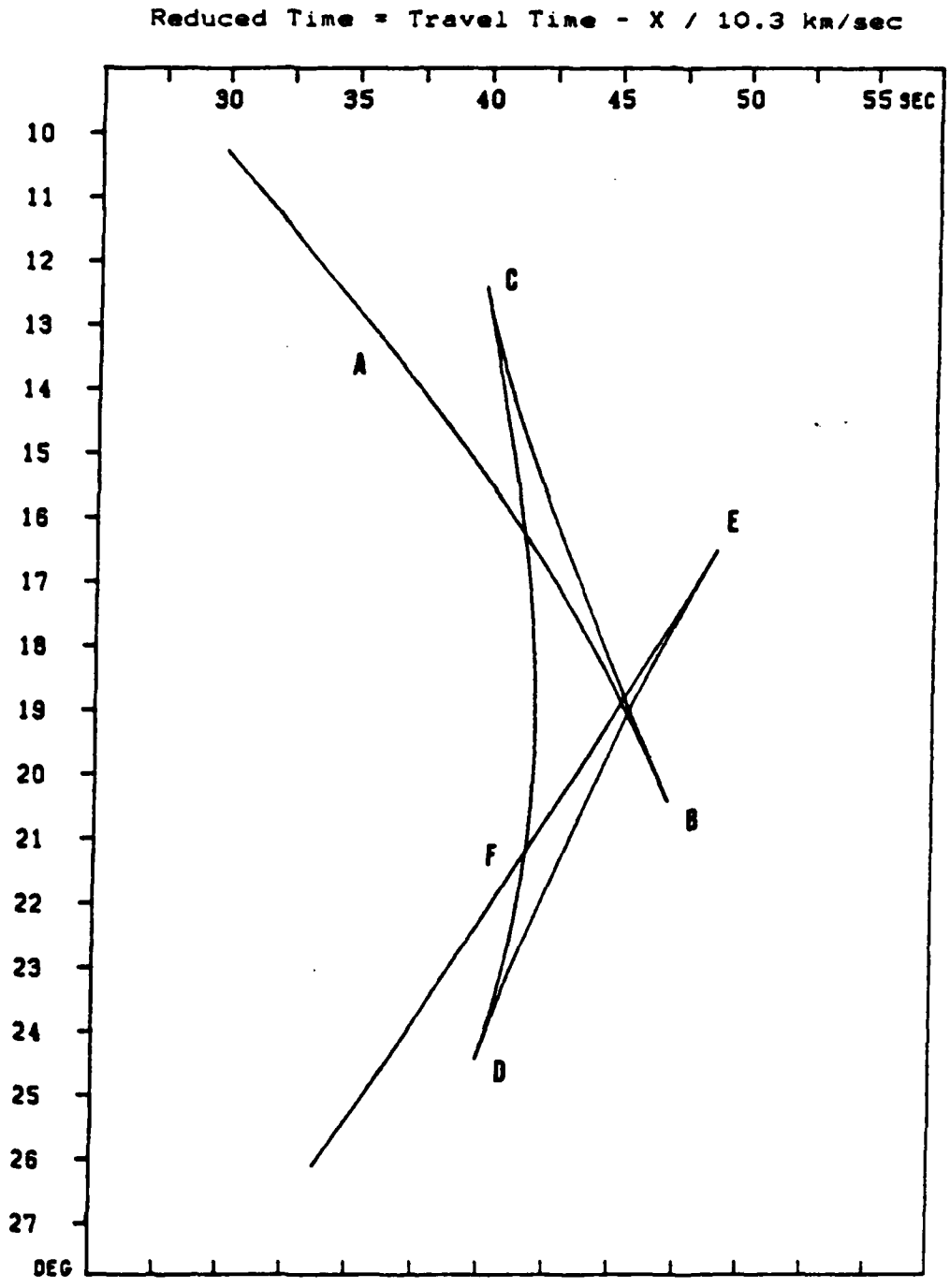

Figure 2a. Reduced travel time curve for the S8 upper mantle velocity model.

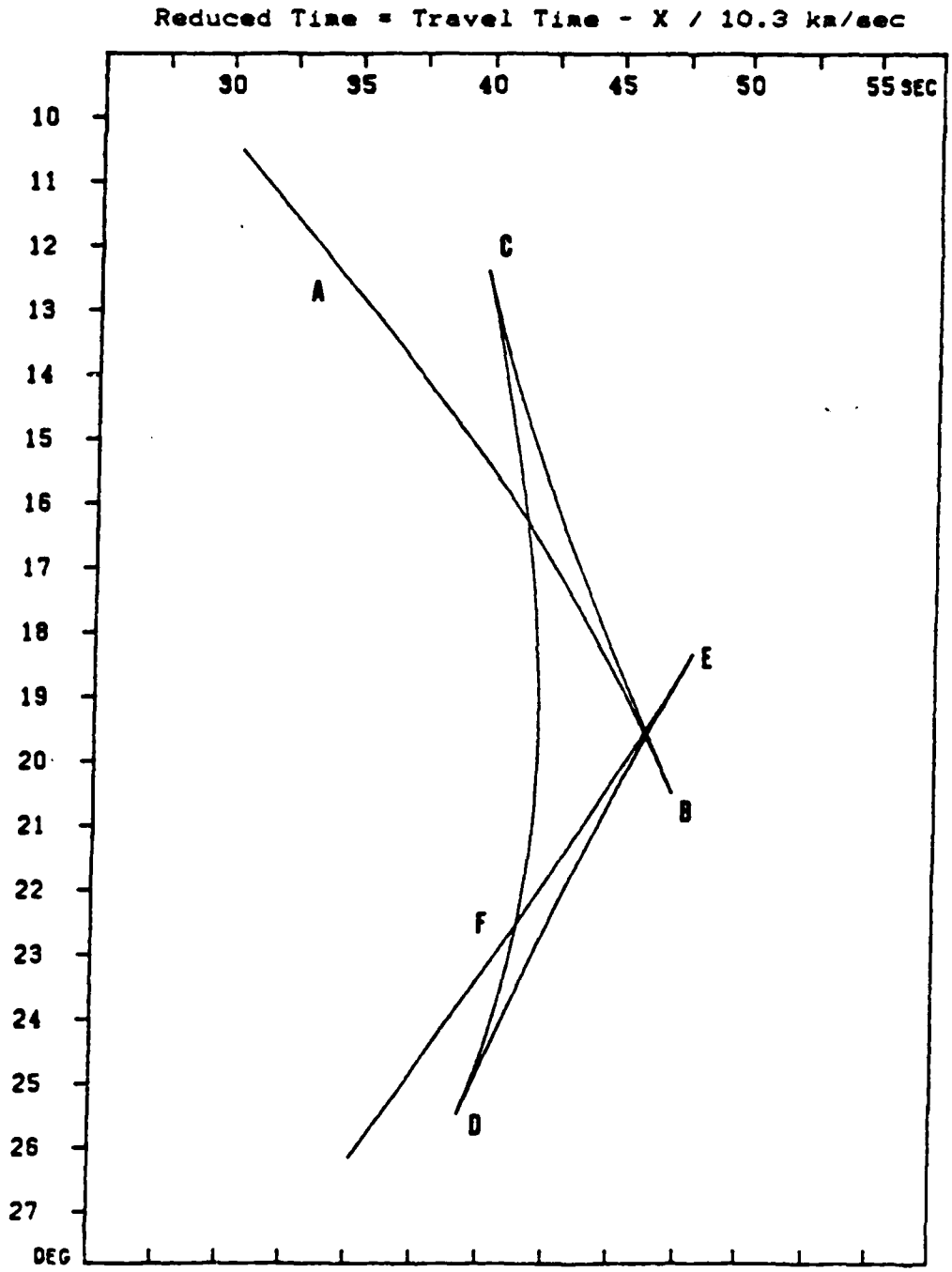

Figure 2b. Reduced travel time curve for the E19 upper mantle velocity model.

model, the synthetic seismogram that we calculated for SCP matched the intermediate-period SCP data almost perfectly.

According to the fault-plane solution of Johnston (1983) for the Hispaniola event, most of the upper mantle stations were located near the P nodal plane. Although the P arrivals are easy to identify and larger than the background noise, some of the apparent interference in the first few seconds of the triplicated waveforms may be spurious arrivals.

SYNTHETIC SEISMOGRAM METHODS

It is reasonable to consider a far-field seismogram as a convolution of a number of operators. For example, the vertical displacement, R(t), is given by:

$$R(t) = E(t) * I(t) * A(t) * S(t) * M(t),$$

where E(t) is the earthquake source time function, I(t) is the instrument response, A(t) is the attenuation operator, S(t) represents the local source and receiver effects, M(t) is the mantle response operator, and * denotes convolution.

Johnston and Langston (1984) determined the earthquake source parameters for the Hispaniola event by moment tensor inversion. The mantle response operator M(t) consists of the set of Green's functions for wave propagation from the Hispaniola event through the mantle velocity model calculated by the WKBJ seismogram method of Chapman (1978). The displacement components, u_i, may be written

$$u_i = -Im \left\{ S(t) * \sum_{t,\theta} \frac{p^{1/2} R(p) K(p)}{\left| d\theta/dp \right|} \right\}$$

where S(t) is the analytic time series,

$$S(t) = s(t) - i\mathcal{H}[s(t)],$$

and

$$S(t) = \frac{M_o}{4\pi} s_f(t) * \frac{\partial}{\partial t}\left[-\frac{1}{\pi\sqrt{2r}} \frac{H(t)}{t^{1/2}}\right]$$

and $\Theta(p) = pr + 2\int_0^z \left(\frac{1}{v^2} - p^2\right)^{1/2} dz$.

We define the following variables:

p = ray parameter,

$\mathcal{R}(p)$ = product of reflection and transmission coefficients,

K(p) = source radiation pattern,

$s_f(t)$ = far-field time function,

Z = ray bottoming depth, and

r = horizontal distance from source to receiver.

We represent the earthquake source time function, instrument, attenuation, and local source effects by a teleseismic wavelet. This method assumes, of course, that at teleseismic distances the earth's response to a propagating wave is a delta function. The observation that the Hispaniola teleseismic (vertical component) waveforms (see Figure 3) are remarkably similar at different azimuths and distances validates this assumption. Moreover, Given (1984) and Grand and Helmberger (1984) testify that convolving a representative teleseismic wavelet with mantle impulse responses gives upper mantle synthetics that are comparable to waveforms calculated using theoretical operators.

Several long-period teleseisms for the Hispaniola event are shown in Figure 3. During the first 20 seconds of

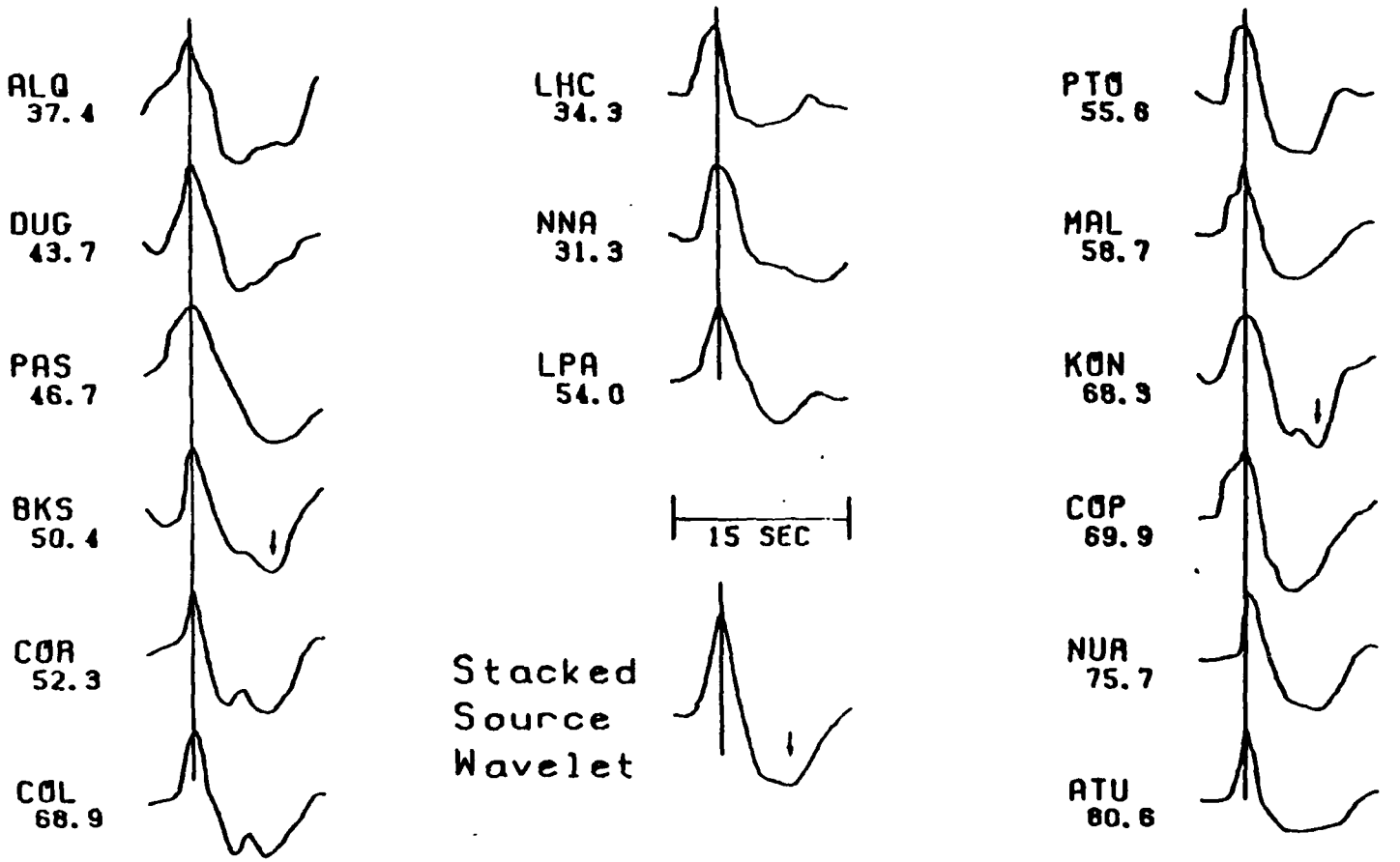

Figure 3. Long-period vertical teleseismic P wave records from the Hispaniola event, and the stacked source wavelet. The wavelets are aligned, summed, and averaged to form the source wavelet. The arrival marked by arrows is a reflection off the base of the low-velocity zone. Numbers are source-to-station distances in degrees.

each record, two distinct pulses arrive. Direct P is consistently followed after about 7 seconds by an event with reversed polarity. Johnston interpreted the second event as an upgoing ray from the source that reflects off the bottom of the low-velocity zone, then travels a path similar to that of P. To make this interpretation, Johnston reconstructed the waveforms by convolving the earth response to the two rays (calculated using Generalized Ray Theory) with the appropriate instrument, earthquake source time function, and attenuation operators. The interaction of P and the 7-second phase constitutes the local souce effects operator.

The source wavelet operator used to model long-period data is a stack of 15 long-period vertical-component teleseisms (Figure 3). Steps taken to construct the wavelet were: 1) align the peaks of the first arrival of each teleseism, 2) normalize amplitudes of each teleseism to the amplitude of the first peak, 3) average the traces. Reversing the polarity of the LHC trace allowed its inclusion in the waveform stack.

Without intermediate-period teleseismic records to make a source wavelet, the interaction between P arrivals and the 7-second arrival cannot be modeled at upper mantle stations for intermediate-period data. In the distance range where intermediate period records are available (22° to 24°), however, triplicated P phases all arrive within the first 3 seconds (see Figures 2a and 2b) after the onset of P. The

synthetics calculated to model these data resulted from convolution of the mantle response and DWWSSN instrument operators and a source time function. E(t) in this case is a Brune time pulse that is 3 seconds long, as Johnston's (1983) source mechaniam study determined.

Included in the long-period source wavelet is the attenuation that teleseismic waves suffer. An additional attenuating operator was not included. Intermediate-period synthetics were not attenuated at all; the effect of attenuation is implicitly included in the assumed source function.

RECEIVER FUNCTION

In this study, as in other upper mantle waveform studies, a delta function represents the effect of shallow structure beneath the receiver. The receiver structure is generally not known. Assuming that it has no effect on wave propagation in this case simplifies the effort of calculating synthetic seismograms.

Of course, this assumption is valid only for stations whose crustal structure does not create arrivals that are obvious on the P records. It requires stations at which converted phases and reverberations in the crust are not strong enough to complicate the upper mantle waveforms. Of the WWSSN stations that recorded the Hispaniola event, Burdick and Langston (1977) suggest that only MNT (Montreal, Canada) may be underlain by crust with sharp velocity contrasts that cause important crustal phases.

To determine whether a delta function closely approximates the receiver function of each of the upper mantle stations used here, the reasoning of Burdick and Langston applies. The presence of SV energy, indicating that crustal phases are interfering with the vertical P waveform, is evident on the radial-component record. If the P waveforms on the vertical- and radial-component records are similar, then the receiver crust is "transparent" (p. 1703, Burdick and Helmberger, 1978) to propagating waves, and the

delta function is appropriate. If the horizontal components do not resemble the vertical, then the crustal structure contains sharp velocity contrasts whose effects on wave propagation cannot be ignored. In such a case, the complications in the vertical P waveform are not due simply to upper mantle structure.

RSCP's horizontal components were rotated into radial and tangential directions. MNT, OTT, and PAL are all within 11° of due north of the source; thus, they are nearly naturally rotated. Radial and vertical components in each case do not differ markedly. The tangential components are of very low amplitude, indicating that little SH energy is generated in the receiver crust.

For the purpose of this study, digitizing and rotating the horizontal components for the remaining stations are unnecessary. The NS and EW components for each station (except SCP) are similar enough to each other, and to the vertical component, that no station was discarded.

The NS-component intermediate-period record for SCP is not available. While the long-period data encourage us that SCP's crustal structure is acceptable, crustal phases should be less obvious on long-period records than on short-period records (Burdick and Helmberger, 1978, and Given and Helmberger, 1980). For the first 3 to 5 seconds, the intermediate-period EW record for SCP is identical to the vertical, however, indicating insignificant crustal features.

TECHNIQUE AND RESULTS

Analysis of upper mantle P waveforms is at the heart of this study. We interpret the observed waveforms by constructing synthetics meant to predict features in records from each station and then comparing the fit between the two. Determining the quality of the fit of predictions to observations is strictly subjective. We pay particular attention to the following features of the waveforms: 1) travel time of first arrival, 2) relative timing of subsequent arrivals, 3) relative amplitudes of pulses, 4) widths of pulses, and 5) polarities of pulses.

For all stations, except BLA and SHA, S8 predicts synthetics that begin 2 to 4 sec earlier than the observed pulses. At BLA the synthetic waveform starts only one second early. Start times for SHA and BLA, at 21.38° and 21.39° respectively, are separated by almost 3 sec. The event on the SHA photographic record begins right at the overlap: thus the discrepancy between the SHA and BLA start times may well be due to error in digitizing the SHA record. Figure 4 shows representative long-period S8 synthetics.

The waveform calculated to match BEC (Figure 5) recovers the fundamental shape of the observation. The relative amplitudes of the troughs and peaks in the entire record are correct, although the first trough is slightly narrow and the first peak is slightly wide.

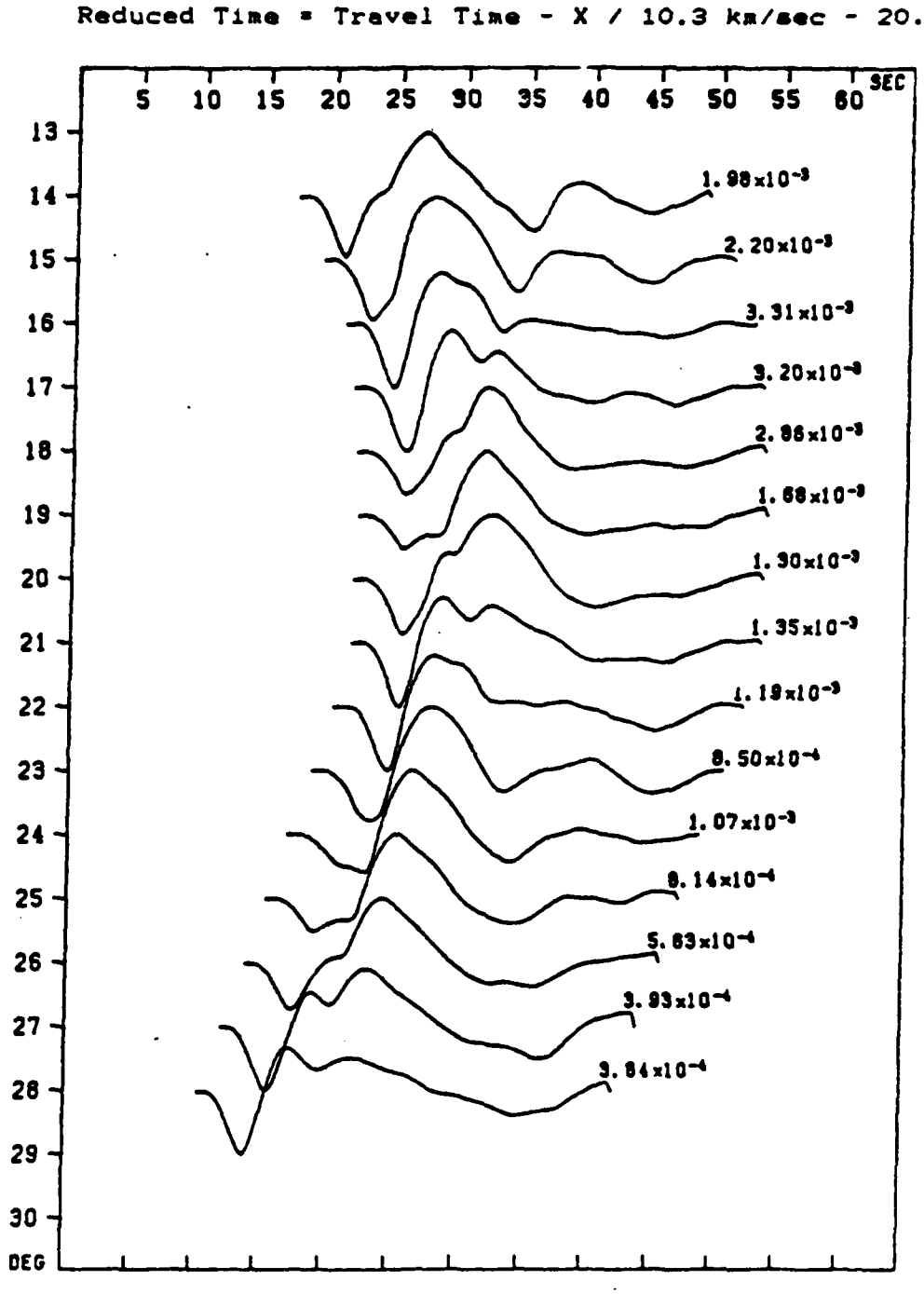

Figure 4. Long-period synthetic seismograms calculated for S8. Absolute travel times are reduced by 10.3 km/sec and advanced by 20 sec. Amplitudes of traces are normalized; maximum amplitudes of traces are shown.

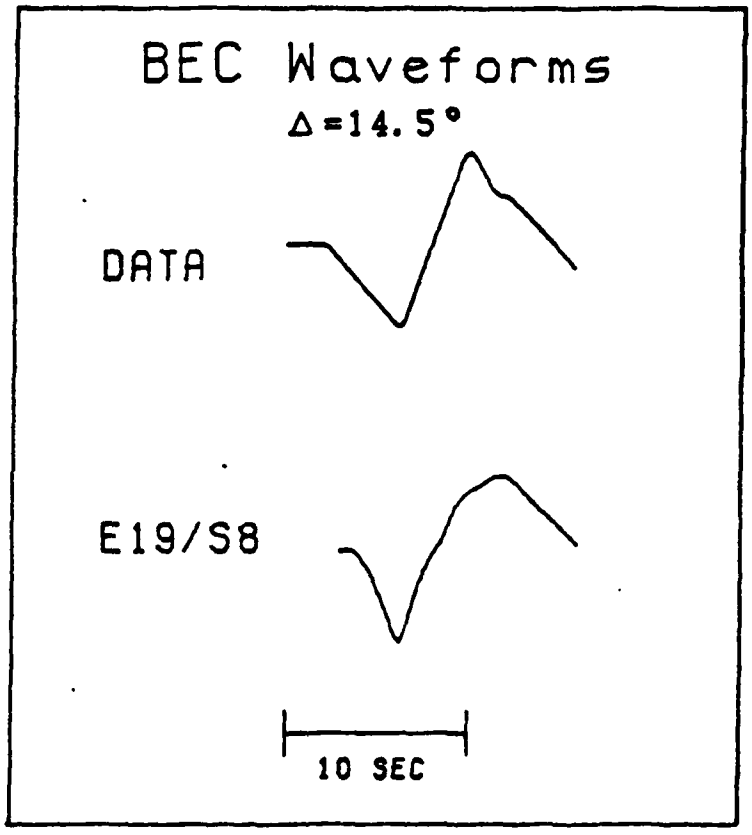

Figure 5. Data and synthetics for BEC.

For both SHA and BLA (Figure 6), the relative timing and widths of peaks are reasonable, but the relative amplitudes need adjustment. The PAL (Figure 6) prediction is excellent. Excessive delay of the first upswing distends the first trough in the long-period SCP record; the first peak fits the data nicely. In the intermediate-period SCP seismogram (Figure 7) the pulses interfere with each other less than they do in the long-period record; we can see the shortcomings of S8 more clearly. The second trough is delayed by 1.5 sec, broadening the first peak. Furthermore, the amplitude of the first wavelet is too small. S8 severely distorts waveforms between 27° and 27.6° (see Figure 8). Indeed, the double peak mimics that of the observations, although the double trough is missing. Our investigation shows that the first peak is actually the pulse that broadens the first trough in the observations; S8 predicts that the amplitude of the first peak is much too large. On close inspection of the 27-degree records, we observe the second pulse moving back in time as distance increases, and changing from a trough to a hump on the left side of the large upswing. We eventually discover that the second peak in the data is not a triplicated direct P phase at all.

Since S8 predicts BEC well enough, we have no grounds for changing the upper 400 km of the starting model. On the other hand, changing the model can improve its performance in the 21- to 28-degree range.

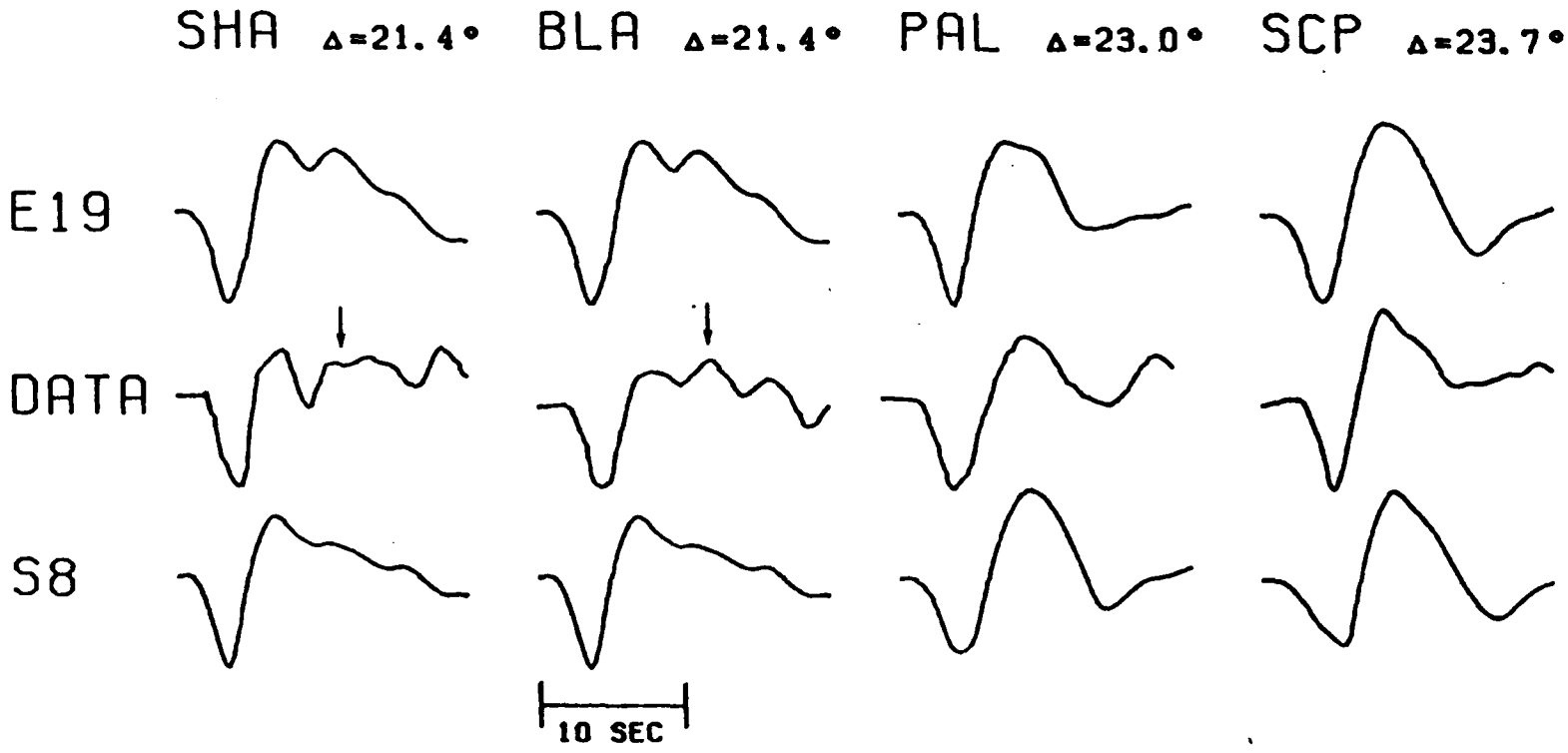

Figure 6. Long-period data and synthetics from 21° to 24°. Arrows on the SHA and BLA observations mark arrivals from the vicinity of the 400-km discontinuity.

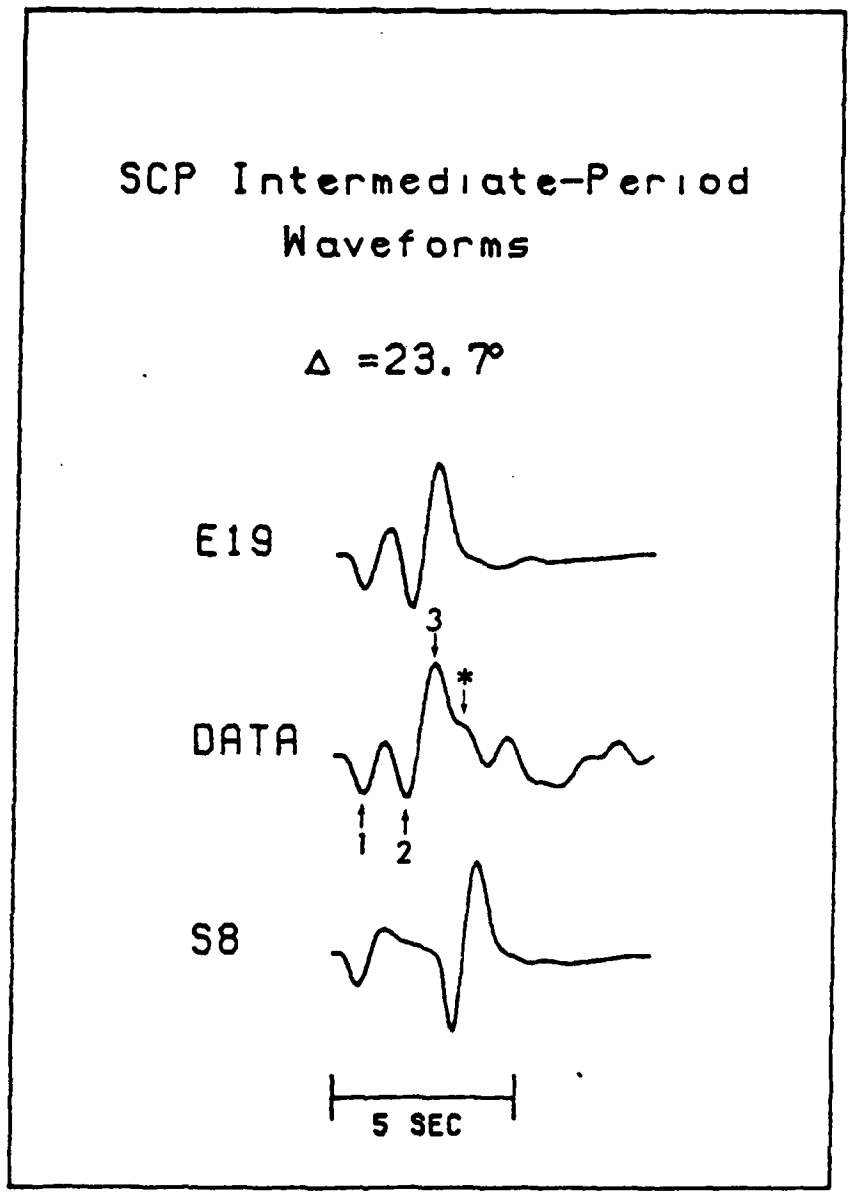

Figure 7. SCP intermediate-period data and synthetics. Pulses represent arrivals of rays that 1) turned just below the 670-km discontinuity, 2) turned just above it, and 3) traveled through it.

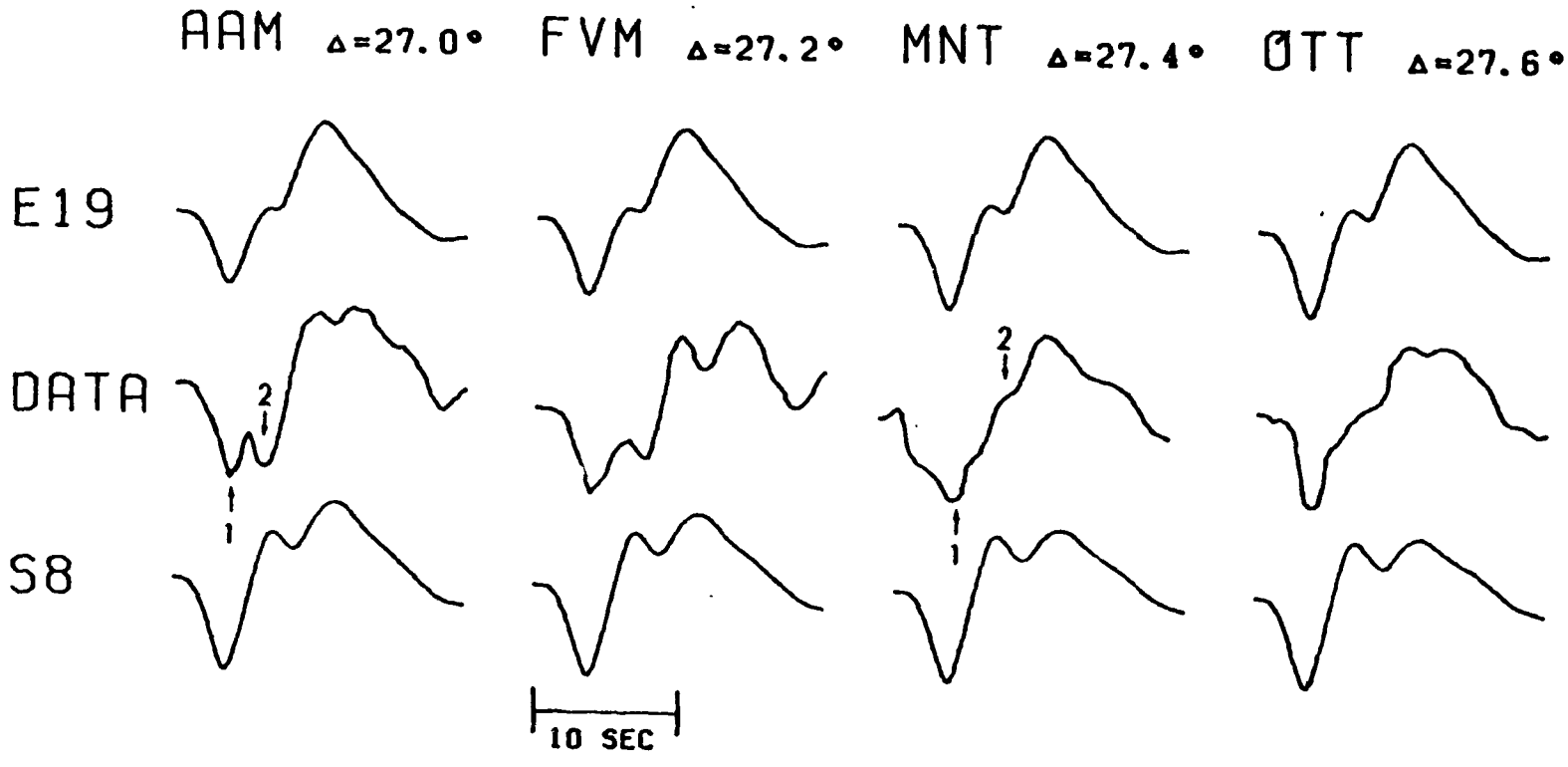

Figure 8. Long-period data and synthetics from 27.00 to 27.60. Our assumptions do not predict the second large peak at AAM, FVM, and OTT. Arrows mark pulses that arrivals of rays from 1) just below the 670-km discontinuity, and 2) just above and within the discontinuity.

A quick look at the S8 waveforms in Figures 4 and 9 suggests that the observations resemble synthetics at distances about 1.5° closer to the source. For example, SCP (23.7°) looks like the 22-degree waveform, and FVM (27.2°) looks like that at 26°.

Waves that arrive at stations between 21° and 28° have bottomed below the 400-km discontinuity. For this reason we attempt to modify the lower half of the velocity profile. We suggest that by shifting the 650-km triplication (DEF) along the 10.3-km/sec branch we will not only systematically delay travel times, but also, we will change the relative timing of arrivals.

At a point to the right of F in Figure 2a, the shift will: 1) delay all arrivals, 2) change the relative timing of arrivals and, in particular, advance the CD branch with respect to the EF branch, and 3) compress the entire triplicated pulse.

To shift and reshape the 650-km triplication branches, we will adjust the starting velocity profile in the following ways:

1) lower the 650-km discontinuity to shift the triplication out in distance,
2) vary the gradient above and below the discontinuity, and change the absolute size of the discontinuity to distort the triplication, and

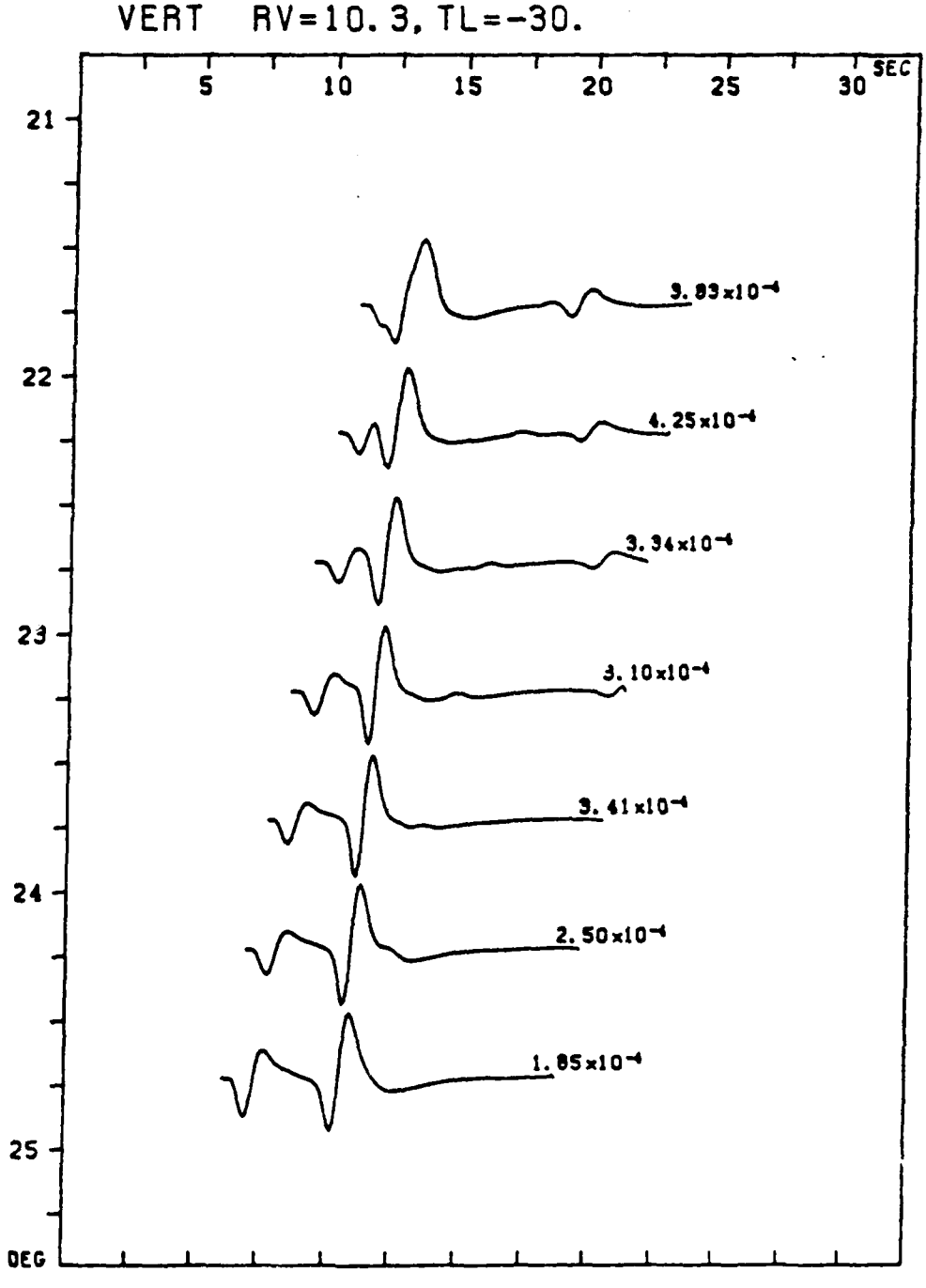

Figure 9. Intermediate-period synthetic seismograms calculated for S8. Absolute travel times are reduced by 10.3 km/sec and advanced by 30 sec. Note that the SCP IP observation resembles the S8 synthetic at 22.25°.

3) sharpen or smooth the discontinuity to lengthen or shorten the duration of the triplication.

We manipulate the starting model according to these guidelines until we achieve a velocity profile whose synthetics satisfactorily match the data. The resulting model will represent only one combination of these activities, however. Since different combinations will shape profiles that predict the observations as well, we conclude that our model is not unique.

Our strategy is to adjust the model so that it fits the SCP intermediate-period (IP) record (Figure 7). At this range, direct P arrivals are separated by about 1 to 2 sec. A time separation of this order is resolvable on the IP record. This record is so clean and noise free that we can calculate synthetics that almost duplicate it. Once we have established this one data point on the travel time curve, we proceed to fit the remaining observations as closely as possible. Representative waveforms for the new model are shown in Figure 10. S8 and the new velocity model E19 are listed in Table 1.

The 400-km Discontinuity. Stations located between 12° and 20° from the source are in an excellent position to record triplicated P arrivals from the vicinity of the 400-km discontinuity. Of the stations whose records are available for this study, only BEC at 14.5° falls in this range. The S8 model predicts a waveform that fits the BEC observation

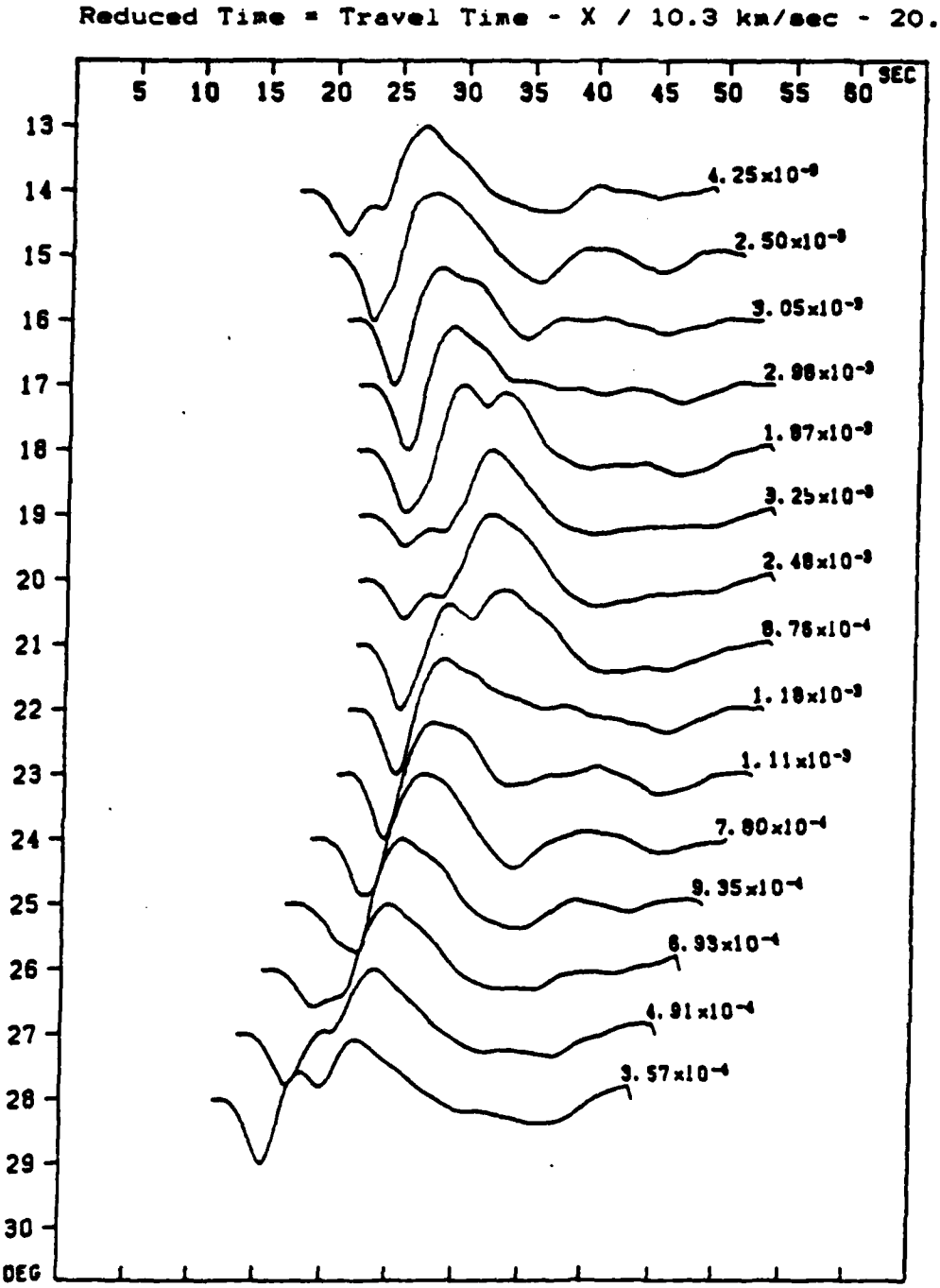

Figure 10. Long-period synthetic seismograms calculated for our model E19. Absolute travel times are reduced by 10.3 km/sec and advanced by 20 sec.

Table 1. S8 and E19 P Velocity Models.

Depth	S8	E19
30.0 km	6.50 km/sec	6.500 km/sec
50.0	7.10	7.100
60.0	8.10	8.100
65.0	8.20	8.200
75.0	8.24	8.240
135.0	8.26	8.260
175.0	8.30	8.300
245.0	8.44	8.440
390.5	8.81	8.810
400.0	9.25	9.250
600.0		10.000
615.0	10.07	
625.0	10.11	10.175
645.0	10.25	
650.0	10.76	
660.0		10.225
667.5		10.275
672.5		10.350
675.0		10.400
675.1		10.650
680.0		10.700
690.0		10.775
705.0		10.850
805.0		11.060
905.0	11.26	11.260

acceptably well. The lack of observations from this distance range is troubling, however. Fortunately, observations of the AB branch (Figure 2) beyond 21° help to confirm that the triplication caused by the upper discontinuity in the S8 velocity model satisfies the data.

From 21° to 24°, the spread between the AB and CD branches of the triplication increases from 6 sec to 9 sec. The position of the AB branch in this range represents the travel time of a diffracted arrival from just above the 400-km discontinuity. The WKBJ method predicts too large an amplitude for this pulse because it is beyond the B cusp. Despite this, its travel time is information that we can use. Before the pulse from the 400-km discontinuity arrives, of course, we see arrivals from the lower discontinuity. At BLA and SHA the arrival of interest causes the second peak in the waveform. By 23° at PAL and 23.7° at SCP (long-period record), the amplitude of the arrival has decreased abruptly and the AB branch has moved back in time. The disappearance of the AB branch is evidence that the first triplication should be no larger than it is.

The 670-km Discontinuity. Our model predicts absolute travel times to within 1 sec at all stations except SCP, SHA, and RSCP. We overestimate the travel time at SCP by 2 sec, and underestimate at SHA by 2.5 sec and at RSCP by 3.5 sec. Perhaps the blame for the SHA misfit lies in error in digitizing the record, as we mentioned earlier.

Waveform fits to BLA and SHA are very good. The first cycle of the waveform is slightly broader than the source wavelet. The pulse from just above the 670-km discontinuity is followed after 1 sec by the pulses that propagate through the discontinuity and along the underside of it (Cormier and Choy, 1981). The second peak is closely matched by a pulse that we predict arrives from the vicinity of the 400-km discontinuity. Our assumptions are not complete enough to explain the slight discrepancy in relative amplitydes between SHA and BLA. The azimuthal separation between these two stations with respect to the source is 25°.

Across the CD-EF intersection at SCP, the intermediate-period synthetic fits the observation almost exactly. The travel time curve indicates a time spread between the EF branch and the back-branch of slightly less than 2 sec; this is precisely the time spread between the first trough and second peak in the data. We can see each of the three triplication branches despite slight interference among the pulses. The two pulses with negative polarity are arrivals from below the 670-km discontinuity and from just above it, in that order. Smoothing the corners of the discontinuity in the profile assured the correct relative amplitudes. The strong peak is the arrival of a ray that traveled through the discontinuity; this is the only record in which the 90-degree phase-shifted pulse from the back-branch is directly obaervable. The hump on the right

side of the peak (* in Figure 7) is not modeled by our assumptions.

The quality of waveform fits at AAM, FVM, MNT, and OTT is very difficult to judge. Each of these stations is very close to the P nodal plane; we expect the triplicated P arrivals to be of very low amplitude. Nevertheless, they are distinguishable from noise, and vital in confirming the position of the CD branch. The first trough in the synthetics corresponds to the first trough in each of the observations. The relative timing of peaks and troughs that our model predicts agrees well with the data. The relative amplitudes of the first trough and second peak are almost exact in each case. The amplitude of the first peak, however, is slightly high, especially at AAM and FVM. The first trough is the head wave that travels underneath the 670-km discontinuity. The second pulse, the superposition of the arrivals from just above and within the 670-km discontinuity, follows the first after about 3.5 sec at AAM and 4 sec at OTT. Its advent is marked by the second trough in the AAM and FVM waveforms, and by the top of the shoulder on the left side of the first peak at MNT and OTT. These data constrain the separation of the EF and CD branches. The WKBJ seismogram overestimates the amplitude of the second pulse; these stations are 1.5° to 2° beyond the D cusp.

We have had great success modeling data received at points on the travel time curve that are away from the CD-EF

crossover. Manipulating the model so that it locates the crossover accurately, however, would have required an immense effort. RSCP and PAL are available to help pin down the crossover point. Our synthetics do not fit these two observations satisfactorily. Although we predict the travel time to PAL well, our travel time to RSCP is 3.5 sec early. The RSCP waveform (Figure 11) exhibits a second arrival about 1 sec after the first. Our experience allows us to interpret the broadening of PAL's trough and peak to indicate the same. Based on waveform shapes alone, we conclude that the CD-EF crossover should move closer to the source.

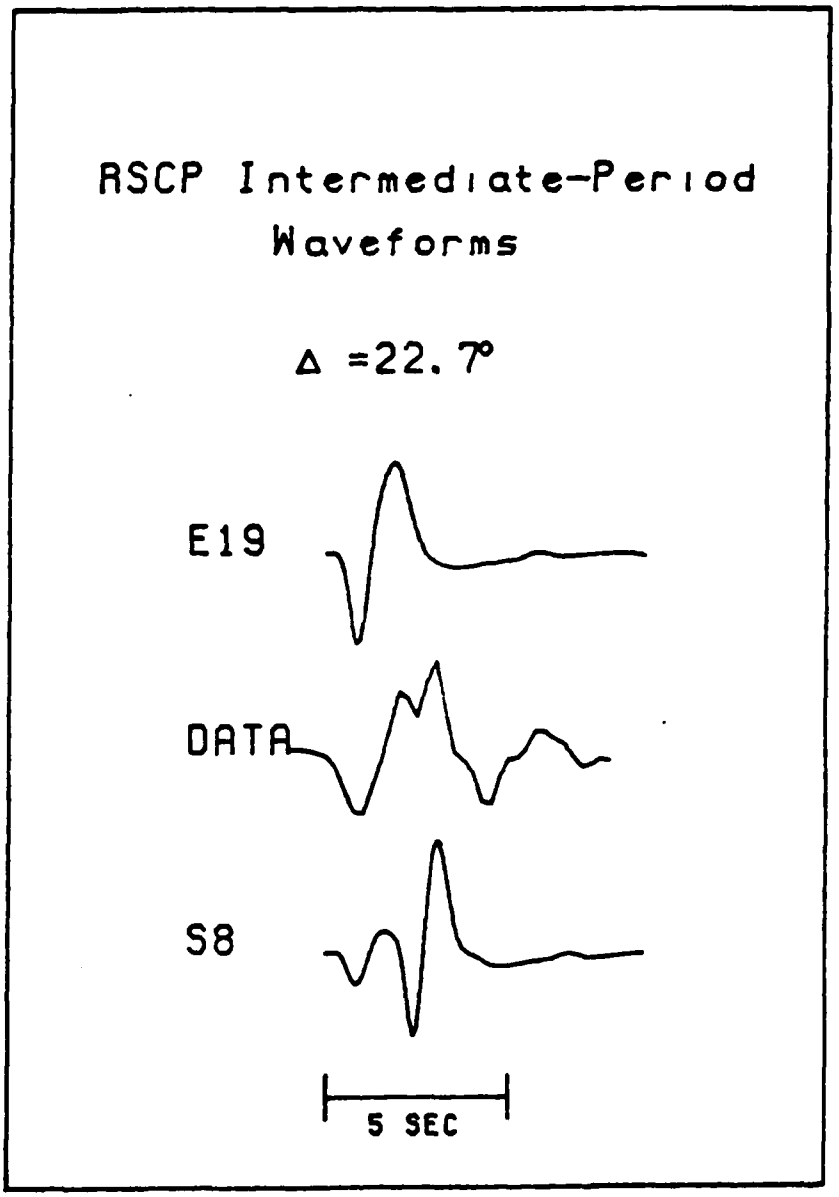

Figure 11. RSCP intermediate-period data and synthetics. Neither model predicts the data. The synthetics appear to be extremely sensitive to the position of the intersection of the CD and EF branches of the travel time curve. We had no success in modeling this observation.

DISCUSSION

Burdick's (1981) model S8 has been modified to satisfy a new set of upper mantle data from eastern North America. The new model is identical to S8 above about 640 km. Features that distinguish the new model from S8 are:

1) the lower discontinuity lies at 670 km instead of at S8's 650 km;
2) velocity gradients immediately above and below the 670-km discontinuity are higher than in S8.

The increased amount of structure resolvable near the 670-km discontinuity, feature 2 above, is a direct benefit of the use of the intermediate-period SCP record. This record was sufficiently noise-free that we were able to reproduce its first 3-4 seconds exceptionally well. Greater availability of such high quality broad-band digital data would no doubt enhance this and similar studies.

The claim of Burdick and other authors that mantle velocity is laterally homogeneous below about 250 km raises questions about the validity of the new model. Does disagreement about the position of the lower discontinuity imply inhomogeneity? Is a difference in position of 20 km at a depth of 650 km resolvable? Could another model satisfy the Hispaniola data?

Given (1984) has recently discussed the two unmentionable unknowns of trial and error inversions for

upper mantle structure: resolution and uniqueness. Using the computer to perform a formal inversion of SH waveforms and travel times for velocity structure, he could quantify the effects of making repeated small perturbations in a starting model. With his insight, we attempt to answer the above questions.

The S velocity profile that Given (1984) derived for the tectonic western U. S. has increases in velocity at about 400 km and 650 km that are much more gradual than any models that have been published since Helmberger and Wiggins (1971) began trial and error inversions of waveforms in short-period observations. His upper velocity change consists of an 8.5% increase spread between 360km and 420 km. Likewise, his lower "discontinuity" is an even more gradual change, a 14% increase between 600 km and 750 km. His model is the simplest that his method allows that satisfies his data. He noted that TNA (Grand and Helmberger, 1984), a recent S velocity model for the same region with truly discontinuous velocity increases, is also a suitable fit to his data. Nevertheless, Given's data set did not allow resolution of sharp discontinuities. We reason, then, that trial and error inversion of data sets of equal or lesser quality to Given's cannot distinguish differences of 20 km in the position of a change in gradient.

The fact remains that the new model fits the Hispaniola data better than S8 does. The new model is not

unique, however. We noted that particular combinations of gradient steepness, discontinuity depth, and velocity jump would satisfy the data. The new model is one combination. Other combinations would fit the data as well. Adding more observations would permit others. Even though the average distance spacing of Burdick's observations is 0.5° to 1°, S8 is not unique either. Given expressed the uniqueness problem in trial and error inversions in this way; "the difficulty of finding a velocity model that satisfied the data is implicitly used as an argument that the model was unique" (p. 55).

REFERENCES

Burdick, L. J. (1981). A comparison of the upper mantle structure beneath North America and Europe, J. Geophys. Res. 86, 5926-5936.

Burdick, L. J., and D. V. Helmberger (1978). The upper mantle P velocity structure of the western United States, J. Geophys. Res. 83, 1699-1712.

Burdick, L. J., and C. A. Langston (1977). Modeling crustal structure through the use of converted phases in teleseismic body-wave forms, Bull. Seism. Soc. Am. 67, 677-691.

Cara, M. (1979). Lateral variations of S velocity in the upper mantle from higher Rayleigh modes, Geophys. J. 57, 649-670.

Chapman, C. H. (1978). A new method for computing synthetic seismograms, Geophys. J. 54, 481-518.

Cormier, V. F., and G. L. Choy (1981). Theoretical body wave interactions with upper mantle structure, J. Geophys. Res. 86, 1673-1678.

Given, J. W. (1984). Inversion of body-wave seismograms for upper mantle structure, Ph. D. Thesis, California Institute of Technology, Pasadena, California.

Given, J. W., and D. V. Helmberger (1980). Upper mantle structure of northwestern Eurasia, J. Geophys. Res. 85, 7183-7194.

Grand, S. P., and D. V. Helmberger (1984). Upper mantle shear structure of North America, Geophys. J. 76, 399-438.

Helmberger, D. V. (1973). Numerical seismograms of long-period body waves from seventeen to forty degrees, Bull. Seism. Soc. Am. 63, 633-646.

Helmberger, D. V., and L. J. Burdick (1979). Synthetic seismograms, Ann. Rev. Earth Planet. Sci. 7, 417-442.

Helmberger, D. V., and G. R. Engen (1974). Upper mantle shear structure, J. Geophys. Res. 79, 4017-4028.

Helmberger, D. V., and R. A. Wiggins (1971). Upper mantle structure of midwestern United States, J. Geophys. Res. 76, 3229-3245.

Johnston, D. E., and C. A. Langston (1984). The effect of assumed source structure on inversion for earthquake source parameters: the eastern Hispaniola earthquake of 14 September 1981, Bull. Seism. Soc. Am. 74, 2115-2134.

Wiggins, R. A., and D. V. Helmberger (1973). Upper mantle structure of the western United States, J. Geophys. Res. 78, 1870-1880.